DEPARTMENT OF DEFENCE
DEFENCE SCIENCE & TECHNOLOGY ORGANISATION
DSTO

DSTO

# Assessment of NASTRAN and PAFEC F-111 WPF FE Models for Elastic Notch Strain Determination at FFVH #13 and FFVH #14

M. Burchill and M. Heller

DSTO-TR-0949

# Assessment of NASTRAN and PAFEC F-111 WPF FE Models for Elastic Notch Strain Determination at FFVH #13 and FFVH #14

*M. Burchill and M. Heller*

**Airframes and Engines Division**
**Aeronautical and Maritime Research Laboratory**

DSTO-TR-0949

**ABSTRACT**

The current AMRL PAFEC and NASTRAN F-111C wing pivot fitting (WPF) finite element (FE) models have been compared to assess their suitability for use in structural integrity investigations, relating to elastic notch strain predictions, at the two critical fuel flow vent holes (FFVHs). Here a comparison is made between the predicted elastic strains and the measured strain data obtained from a full scale wing test. It was found that the PAFEC model accurately predicts the strain distribution around FFVH #13, however it incorrectly predicts significantly higher strains in FFVH #14 and greater bending of the wing skin above FFVH #14. In contrast, the NASTRAN model gives accurate results for the large stress gradient around both FFVH #13 & #14, and upper plate bending, when higher order 'p' elements are used. Hence it is considered that while FE analyses of FFVH #13 in the F-111 WPF can be accurately completed with either the current PAFEC or NASTRAN model, only the latter is suitable at FFVH#14. Hence the NASTRAN model is the recommended model for general elastic WPF structral integrity assessments, and continued development where appropriate.

*Published by*

*DSTO Aeronautical and Maritime Research Laboratory*
*PO Box 4331*
*Melbourne Victoria 3001 Australia*

*Telephone: (03) 9626 7000*
*Fax: (03) 9626 7999*

*AR-011-233*
*March 2000*

**APPROVED FOR PUBLIC RELEASE**

# Assessment of NASTRAN and PAFEC F-111 WPF FE Models for Elastic Notch Strain Determination at FFVH #13 and FFVH #14

## Executive Summary

AMRL has been investigating for some time fatigue cracking in the wing pivot fitting (WPF) of the F-111C aircraft in service with the RAAF. The WPF contains a number of 'hot spots', such as some of the open fuel flow vent holes near the wing root, e.g. Fuel Flow Vent Hole numbers 13 and 14 (FFVH #13, FFVH #14). Historically most effort has been directed at FFVH #13, however recently there has been concern about FFVH #14 as well. Continuing structural integrity assessments at these locations are in progress, and here the use of Finite Element (FE) models plays an active role. Of particular relevance is that previous stress analyses of FFVH #13, including rework profile analysis, have been performed using a PAFEC FE model. While this PAFEC model produces accurate strain results around FFVH #13, some doubts exist regarding the accuracy of the strain predictions around FFVH #14. This is of particular interest since it appears that FFVH #14 may be the next most critical fuel flow vent hole after FFVH #13. Recently a significantly more enhanced NASTRAN 3D model has been received by AMRL from the Original Equipment Manufacturer in support of our sole operator status. The new NASTRAN model may potentially be more suitable than the current PAFEC model for meeting our FE modelling requirements at locations such as FFVH #14 and the wing pivot fitting in general. Hence a decision needs to be made concerning whether the PAFEC model is adequate or warrants further development, or whether effort needs to be directed solely at the new NASTRAN model.

In the present work the current AMRL PAFEC and NASTRAN F-111 WPF FE models have been compared to assess their suitability for use in structural integrity investigations, relating to elastic notch stress and strain predictions, at the two critical fuel flow vent holes. Here a comparison is made between the predicted elastic strains and measured strain data obtained from a full scale wing test. It was found that the PAFEC model accurately predicts the strain distribution around FFVH #13, however it incorrectly predicts significantly higher strains in FFVH #14 and greater bending of the wing skin above FFVH #14. In contrast the NASTRAN model gives accurate results for the large stress gradient around both FFVH #13 & #14, and upper plate bending, when higher order 'p' elements are used.

It is recommended that only the NASTRAN model should be used for F-111C FFVH #14 assessments. This model is also considered the preferred model for general elastic WPF structral integrity assessments, and continued development where necessary. The current version of the PAFEC model is only recommended for assessments at FFVH #13.

# Authors


## Madeleine Burchill

Airframes and Engines Division


*Madeleine Burchill graduated from the Royal Melbourne Institute of Technology in 1992 with a Bachelor of Engineering (Aero). She commenced employment with the Aeronautical and Maritime Research Laboratory in 1994 first as a contract engineer, then in 1996 as a Professional Officer. From 1994-1997 she was involved in investigating the dynamic response of gearboxes and engines in both Australian Defence Force and commercial aircraft. Currently she has been using advanced Finite Element methodologies, such as non-linear and optimisation algorithms, to research fatigue critical components of the F-111.*


## Manfred Heller

Airframes and Engines Division


*Manfred Heller completed a B. Eng. (Hons.) in Aeronautical Engineering at the University of New South Wales in 1981. He commenced employment in Structures Division at the Aeronautical Research Laboratory in 1982. He was awarded a Department of Defence Postgraduate Cadetship in 1986, completing a PhD at Melbourne University in 1989. His work has focussed on the areas of stress analysis, fracture mechanics and fatigue life extension methodologies. Since 1992 he has led tasks which develop and evaluate techniques for extending the fatigue life of ADF aircraft components. He is currently a Senior Research Scientist in the Airframes and Engines Division, Aeronautical and Maritime Research Laboratory, DSTO.*

# Contents

# 1. Introduction

For some time AMRL has been investigating fatigue cracking in the wing pivot fitting (WPF) of the F-111C aircraft in service with the RAAF. The WPF contains a number of 'hot spots', such as some of the open fuel flow vent holes near the wing root, for example, fuel flow vent hole number 13 and 14 (FFVH #13, FFVH #14). Figures 1, 2 and 3 show schematically, the locations of these fatigue critical components in the WPF of the F-111. Historically most effort has been directed at FFVH #13, however recently there has been concern about FFVH #14 as well. Cracking at these locations is understood to be dependant upon loading under normal RAAF usage, and the residual stresses from the Cold Proof Load Test (CPLT) [1]. The CPLT, performed periodically on the F-111 airframe, subjects the structure to extreme conditions (-40°C) and limit loading (-2.4g to +7.33g), which certifies that the airframe contains no flaws above a certain size. During the CPLT, local compressive plastic deformation occurs at FFVH #13 and #14, resulting in large tensile residual stresses at a particular position, on the hole boundary. Fatigue cracking then occurs at these locations, when the effects of the large tensile residual stresses from the CPLT are compounded by the normal flight loading.

Continuing structural integrity assessments at these locations are in progress, and these are based on the use of finite element (FE) models and full scale fatigue tests. Here in particular the FE approach can be used to: (i) determine and assess rework profiles which remove cracks, while reducing the peak stress concentration [2, 3], (ii) perform non-linear material analysis to determine detrimental residual stresses, (iii) provide other required inputs necessary to undertake durability and damage tolerance assessments, including crack growth models. Of particular relevance is that previously stress analyses of FFVH #13, including rework profile analysis, have been performed using a PAFEC FE model [4]. This PAFEC model was converted and developed from a NASTRAN data deck supplied by the Original Equipment Manufacturer (OEM). An extensive development phase of this model included refinement of the element mesh around FFVH #13 and the development of a constitutive material model for plastic analysis. This PAFEC model produces accurate strain results around FFVH #13.

However, some doubts exist regarding the accuracy of the strain predictions from the PAFEC FE model for FFVH #14. This is of particular interest since it appears that FFVH #14 may be the next most critical fuel flow vent hole, after FFVH #13. Recently a significantly enhanced NASTRAN data deck has been received by AMRL from the OEM [5], in support of our sole operator status. The new NASTRAN model, may prove to be more suitable than the current PAFEC model for meeting our FE modelling requirements, at locations such as FFVH #14, and the WPF in general. Hence a decision needs to be made concerning whether the PAFEC model is adequate or warrants further development, or should our effort be directed at the new NASTRAN model.

This *technical report* investigates and documents the capacity of either model to fulfil AMRL FE analysis requirements around FFVH #13 and #14, for determining elastic

strains. In particular, a comparison is made between the elastic strains each model predicts, and where appropriate, with measured (elastic) strain data from a full scale wing test. Here, localised regions around the two FFVHs and in the surrounding WPF structure are considered. It should be noted that an accurate elastic model is also a key requirement for potential elastic/plastic analyses.

# 2. PAFEC Finite Element Model

The current AMRL PAFEC FE model, shown in Figure 4a, is a derivation of an original General Dynamics (OEM) F-111 Stub Wing FE model, which was converted at AMRL from a NASTRAN data deck using the NAPEC code. A substructure model, of the critical fatigue region around FFVH #13, that had previously been used by AMRL was then incorporated into the above modified model to improve the accuracy of local stress and strain predictions. Figure 5a shows the substructure region, which consists of stiffener #3, the upper wing skin and chordwise stiffener between stiffeners #2 and #4. It should be noted that this substructure model does not include the titanium shear web. The current AMRL PAFEC model has also had further modifications to both the stub wing and substructure regions. Comprehensive details regarding the development and attributes of the various PAFEC models is given in Reference [4]. However, in the following sections 2.1 and 2.2, a brief description is given of the most important alterations to each of the three (3) models that have been used by AMRL in prior analyses. These models are: (i) Original OEM stub wing NASTAN data deck and Modified OEM PAFEC FE model, (ii) Combined OEM and AMRL PAFEC FE model, and (iii) Current AMRL PAFEC FE model.

## 2.1 Previous PAFEC FE models

To meet AMRL requirements at the time, the original OEM stub wing NASTRAN data deck, was altered considerably after being transformed to a PAFEC model (Modified OEM PAFEC FE model). This original model used the following: 8 noded 3D elements in the upper wing skin and the WPF hub, 4 noded 2D elements for the titanium shear web, stiffeners and other wing skins, and 1D elements were used to enhance the stiffness were applicable. Subsequent AMRL changes to the PAFEC conversion of the original model included, changing the Young's modulus of D6ac steel from 29000ksi to 30023ksi as well as replacing some of the 2D plane stress/plane strain elements, around FFVH #13, with semi-loof elements. Improvements in accuracy were also achieved by coupling the freedoms between the 2D stiffener elements and the 3D wing skin elements and modelling the bolts between the titanium shear web and the stiffener with repeated freedoms. Investigations were also undertaken to assess the model's sensitivity to increasing mesh density around FFVH #13. The model geometry was also adapted to

closely match particular features of the current (at that time) AMRL test article, in particular for the shear web and stiffener around FFVH #13.

The combined OEM and AMRL PAEFC FE model joined a previously developed AMRL PAFEC substructure model of the critical area around FFVH #13, with the modified OEM stub wing model described above. This model uses the loads from the stub wing model as boundary conditions for analysis of the substructure. This combined model was a substantial improvement on the previous version, with improved load transfer through the shear web/stiffener bolts, enhanced mesh refinement around FFVH #13 and improvements to the overall stiffness in specific regions. Here also the order of the elements, in the region in the vicinity of FFVH #13 was increased, with 2D elements being changed from 4 nodes to 8 nodes and 3D elements from 8 nodes to 20 nodes. Furthermore, significant effort was directed at overcoming the compatibility problems in combining two separate models, including re-numbering of nodes and some re-meshing.

## 2.2 Current AMRL PAFEC FE Model

The development and implementation of an AMRL D6ac non-linear constitutive material model, along with the improvements listed above, allowed AMRL to extend the capabilities of the PAFEC model further. Unfortunately, due to the computational size of the model, relative to the computing hardware capability at the time, non-linear material (ie. plastic) analysis of the combined OEM and AMRL PAFEC model could not be completed. Hence to overcome this difficulty, and to improve model accuracy at specific locations such as FFVH #13 (as compared to test results) further modification was undertaken to achieve the Current AMRL PAFEC FE model [4]. Specific alterations included aligning stiffener #3 in the X-Y plane as well as increasing the thickness of stiffener #3 gradually towards the upper plate interface around FFVH #13. Improvements were also achieved by modifying the shape of FFVH #13 and increasing the mesh density both around FFVH #13 and in the nearby wing skin.

The most recent (1999) version of the current PAFEC FE full wing model, *FULLWINGBBEC*, consists of the WPF, the wing sweep actuator structure, the wing pivot hub and approximately 2.3m of the outboard wing assembly and is shown in Figure 4a. Figure 5a shows the smaller substructure model, *BASEE*, of stiffener #3, and a portion of the upper wing skin and hub. A brief summary of the main attributes of these models is given in Table 1, 2 and 3. Typically for iterative plasticity analyses, the sub-model is firstly treated as a part of the 'full'[1] model, and displacements are extracted from the full model results, once the overall elastic analysis is completed. These are then applied to the sub-model as 'prescribed displacements', at the sub-model boundaries and at bolt locations, for subsequent iterations. The highly refined mesh region around FFVH #13 and #14 is shown in Figure 6. Here the shape of FFVH #13 is a representation of the actual test article profile. The upper plates and hub of the WPF are modelled with 3D elements, while 2D elements are used to represent the lower plates and stiffeners. It

[1] 'Full' in this context means the complete PAFEC FE model, not the *entire* wing.

should be noted that the WPF is almost entirely all composed of D6ac steel, with the exception of the titanium shear web. The outer wing is principally modelled with 2D elements of aluminium alloy, where 1D beam elements are used to modify the stiffness. Previously, correlation factors [6] have been determined by comparing the strain results from a wing test strain survey, conducted at AMRL, with the finite element predictions.

The loading applied to the FE model corresponds to the maximum and minimum load applied during the CPLT (+7.33g and -2.4g). It was determined so that the wing root bending moment and shear force are equivalent to the CPLT. Figure 4b and Figure 5b show the loads and prescribed displacements applied to the full and sub-structure model respectively. It should be noted that the sub-modelling method is relatively complex and requires careful control of the substructure boundary nodes and associated displacements due to its semi-automated analysis procedure. To undertake the analyses, the model is processed on a Hewlett Packard series 9000 computer at AMRL, while post-processing is performed in PIGS (PAFEC Interactive Graphic) and PUPPIES (PAFEC User Pre and Post Program for the Interactive Evaluation of Structures).

*Table 1: Features of the current PAFEC substructure and full wing FE models*

| Feature | | Number in substructure model | Number in full wing model |
|---|---|---|---|
| elements | - total | 2877 | 6290 |
| | - 3D | 1050 | 1770 |
| | - 2D | 1827 | 4094 |
| | - 1D | 0 | 426 |
| nodes (structural) | | 10169 | 13496 |
| degrees of freedom | | 37727 | 48426 |
| material types | | 1 | 3 |

*Table 2: Element types used in the current PAFCEC substructure and full wing FE models*

| Model structure | region (both sub and full) | Principle element type |
|---|---|---|
| wing pivot fitting | upper plate | 20 noded 3D isoparametric bricks |
| | lower plate and stiffeners | 4 noded 2D facet thin shells |
| | stiffener #3 only | 8 noded 2D semi-loof curved shells |
| | chordwise stiffener | 8 noded 2D semi-loof curved shells |
| | shear web | 4 noded 2D facet thin shells |
| | hub | 20 noded 3D isoparametric bricks |
| outer wing | stiffeners and plates | 4 noded 2D isoparametric plane stress/strain curvilinear quads |
| | *additional stiffness* | 2 noded 1D beams |

*Table 3: Properties of materials used in the current PAFEC FE substructure and full wing models*

| Material | Principle use | Young's modulus $E$ (ksi) | Poisson's ratio $\nu$ |
|---|---|---|---|
| D6ac | WPF | 30,023 | 0.32 |
| Aluminium alloy | outer wing | 10,700 | 0.33 |
| Titanium alloy | shear web | 16,400 | 0.31 |

# 3. AMRL NASTRAN Finite Element Model

Recently a new large scale NASTRAN WPF FE model has been provided to AMRL, by the RAAF and the OEM, for use in support of Australia's sole operator status for the F-111 aircraft. While this is a large scale and complex model developed by the OEM, considerable work at AMRL has been undertaken to improve the model, particularly in relation to further improving the accuracy of peak notch stress predictions at various critical locations in the WPF [5]. The model is shown in Figure 7a. There are essentially two versions of this current NASTRAN model; (i) a standard model using 'h' elements and (ii) enhanced model, identical to the standard model except for the use of 'p' or higher order polynomial elements in selected regions. For example at locations having large stress gradients, such as FFVH#13 and #14. In the following sections 3.1 and 3.2 a brief description is given of the most important alterations and features of the AMRL NASTRAN model.

## 3.1 AMRL Development of the OEM NASTRAN FE Model

The current (1999) AMRL NASTRAN FE models have had the forces and moments adjusted to accurately represent the most recent AMRL test article. Here the loading applied in the original FE model to represent the weight of the wing was removed, which enabled the model to mimic the strain gauge response during a typical CPLT, (the gauges are zeroed when the wing is unloaded). As was the case for the PAFEC model, the FFVH #13 shape has been changed to reflect the current test article geometry. Some more recent alterations include the re-modelling of the stiffener #3/Titanium shear web bolts, and considerable refinement of the mesh at the known critical fatigue locations, ie. FFVH #13 and SRO #2. Note that the use of 'p' or higher order elements in the enhanced model, around FFVH #13 and #14 allowed further increases in the accuracy of stress predictions.

## 3.2 Features of the Current NASTRAN Model

Both the standard and enhanced NASTRAN models, namely files *REV1e* and *REV1e.p1* respectively, include a detailed 3D mesh of the WPF, the wing pivot hub, with a portion

of outboard wing structure, as shown in Figure 7a. In Figures 8 and 9, more detail of the finite element mesh for stiffener #3 and around FFVH #13 and #14 is given respectively. The loading applied to the FE model corresponds to the maximum and minimum applied load during the CPLT (+7.33g and -2.4g). It was determined so that the wing root bending moment and shear force are equivalent to the CPLT. Here one single load at the position of one inboard test actuator is applied, along with a combination of bending moment, shear force and torsional load acting at the outermost position on the wing geometric centre (to represent the combined loading of the remaining test actuators). This loading is shown in Figure 7b. A brief summary of the main attributes of the standard NASTRAN model is given in Table 4, 5 and 6. The enhanced NASTRAN model is almost identical to the standard model except in the vicinity of FFVH #13 and #14 where standard 'h' elements have been replaced by the higher order 'p' elements, as shown in Figure 10. It is envisaged that if non-linear material analyses of this model are required, then these 'p' elements will be replaced with an even more dense 'h' element mesh, and solved using the ABAQUS code. To undertake the analyses, the model can be processed on one of two computers available to AED users. For example, the Silicon Graphics IR 10000 machine can process this model in less than half an hour, while several hours are needed to process the elastic model on the AED HP 9000 machine. All pre and post processing is performed using the PATRAN code on the AED HP 9000 machine.

*Table 4: Features of the current NASTRAN FE model*

| Feature | | Number in model |
|---|---|---|
| elements | - total | 44169 |
| | - 3D | 38575 |
| | - 2D | 4731 |
| | - 1D | 843 |
| nodes | | 66581 |
| degrees of freedom | | 200000+ |
| materials | | 43 |
| multiple point constraints | | 65 |

*Table 5: Element types used in the current NASTRAN FE model*

| Model structure region | | Principle element type |
|---|---|---|
| wing pivot fitting | upper plate | 8 noded 3D isotropic bricks |
| | lower plate and stiffeners | 8 noded 3D isotropic bricks |
| | stiffener #3 only | 8 noded 3D isotropic bricks |
| | chordwise stiffener | 8 noded 3D isotropic bricks |
| | shear web | 8 noded 3D isotropic bricks |
| | hub | 8 noded 3D isotropic bricks |
| | boron doublers | 4 noded 2D anisotropic plates |
| outer wing | stiffeners and plates | 8 noded 3D isotropic bricks |
| | *additional stiffness* | 2 noded beams |

*Table 6: Properties of materials used in the current NASTRAN FE model*

| Material | Principle use | Young's modulus $E$ (ksi) | Poisson's ratio $\nu$ |
|---|---|---|---|
| D6ac | WPF | 30,000 | 0.32 |
| Aluminium alloy | outer wing skins | 10,500 | 0.33 |
| Titanium alloy | shear web | 16,000 | 0.32 |
| Composite | boron doublers | defined stiffness matrix | |

# 4. Comparison with Experimental Data for Strains in the Vicinity of FFVH#13 and #14

One way of assessing the quality of a typical FE model is to compare strain predictions to appropriate test data. Since 1990 a number of strain surveys of the F-111 WPF have been performed [8-15], including a full aircraft CPLT and several full wing strain surveys conducted at AMRL. In prior work, the most recent strain data, from the AMRL static test of an ex-USAF starboard wing, was processed to provide elastic[2] results, where the method used is given in Reference 7. Figure 11 shows the locations at which this strain data was measured during the test around FFVH #13 and #14. Hence in this section the accuracy of the two FE models is assessed by comparison with the test data. The following four regions will be discussed, as shown schematically in Figure 11: (i) strip strain gauges around FFVH #13 perimeter which measure the strains around upper outboard and lower inboard corners, which include the locations of peak compressive strain during the maximum CPLT load, (ii) strip strain gauges around FFVH #14 perimeter which measure the strains around upper outboard and lower inboard corners which include the locations of peak compressive strain during the maximum CPLT load, (iii) rosette strain gauges mounted on the forward and aft face of stiffener #3, below FFVH #13 and #14, will give an indication of the load flow and the direction of the principle strains, and (iv) single strain gauges mounted on and under the upper wing skin above FFVH #13 and #14, which will indicate the magnitude of the wing skin secondary bending above the FFVHs. In Table 7 the test gauge number and the closest corresponding FE node number, (where applicable) from each of the models are given.

[2] Linear portion of the incremental test data was extrapolated to the full 100% load

*Table 7: Test strain gauges and corresponding nodes in both the PAFEC and NASTRAN FE models*

| Gauge position and description (as shown in Figure 11) | | Gauge number | Node number | |
|---|---|---|---|---|
| | | | *PAFEC model* | *NASTRAN model* standard |
| 1 | Strain rosette on stiffener #3 under FFVH #14 | 80/84 *(aft/fwd)* | 7487 *(top/bottom)* | 58103/58106 |
| 2 | Strain rosette on stiffener #3 between FFVH #14 and #13 | 79/83 *(aft/fwd)* | 7365 *(top/bottom)* | 63379/63424 |
| 3 | Strain rosette on stiffener #3 under FFVH #13 | 78/82 *(aft/fwd)* | 7333 *(top/bottom)* | 64001/65515 |
| 4 | Strain rosette on stiffener #3 inboard of FFVH #13 | 77/81 *(aft/fwd)* | 7205 *(top/bottom)* | 64071/65589 |
| 5 | Strip (5) strain gauge in lower inboard corner of FFVH #13 | 72 | *N/A** | *N/A** |
| 6 | Strip (5) strain gauge in upper outboard corner of FFVH #13 | 73 | *N/A** | *N/A** |
| 7 | Strip (5) strain gauge in lower inboard corner of FFVH #14 | 75 | *N/A** | *N/A** |
| 8 | Strip (5) strain gauge in upper outboard corner of FFVH #14 | 76 | *N/A** | *N/A** |
| 9 | Single gauge on upper plate above FFVH #14 | 39 | 6641 | 58370 |
| 10 | Single gauge under upper plate above FFVH #14 | 74 | 6396 | 58375 |
| 11 | Single gauge on upper plate above FFVH #13 | 38 | 6461 | 36797 |
| 12 | Single gauge under upper plate above FFVH #13 | 71 | 6397 | 63804 and 63803 |

** strip strain gauges do not coincide with one particular node*

## 4.1 Strain Distribution Around FFVH #13

In previous work a family of FFVH #13 rework profiles was determined by AMRL. Here the aim was to obtain rework shapes which remove cracked material and reduce the peak hole stress concentration due to in-service loading, thus reducing the likelihood of further fatigue cracking. The FFVH #13 profile used in the present investigation is known as 'baseline' or 'standard' profile, determined from the RAAF fleet of F-111 FFVH #13 profiles that have not been reworked, but differ from the blueprint profile due to the confidence cutting and other inspection procedures. Both the NASTRAN and the PAFEC FE models have profiles that are similar to the test articles 'baseline' profile. Figure 12

and Figure 13 show the profiles from both models around FFVH #13 and #14. As can be seen in Figure 12, the profile of FFVH #13 in the PAFEC model is different from both the test article and NASTRAN profile, and this was assumed to be due to inaccurate measurements of the cast made of the FFVH. The non-zero elastic principle strain or 'hoop strain' results, during maximum positive CPLT loading, around the perimeter of FFVH #13 are presented in Figure 14. The peak hoop strains around FFVH #13 are presented below in Table 8, for both the upper outboard and lower inboard corners, noting that service experience indicates that cracking occurs usually at the lower inboard corner.

*Table 8: Peak hoop strain ($\varepsilon_{\theta\theta}$) around FFVH #13 at maximum CPLT load*

| Location | FFVH #13 peak strain (με) | | | |
|---|---|---|---|---|
| | Elastic test results | PAFEC results[3] | NASTRAN results | |
| | | | *standard* | *enhanced* |
| Lower inboard corner | -20147 | -19984 | -11730 | -17316 |
| Upper outboard corner | -12683 | -14437 | -6665 | -11583 |

The PAFEC model accurately estimates the peak strains, in particular the large (greater than material yield in a plastic analysis) strains that occur in the upper outboard and lower inboard corners of FFVH #13. The precision of the PAFEC model around FFVH #13 has been validated previously through a rigorous calibration and correlation procedure [4]. The PAFEC FE results presented in Figure 14 and Table 8 have been multiplied by the recommended correlation factor [6]. The results from elastic analysis of both the standard and enhanced NASTRAN models show a similar trend around the perimeter of FFVH #13, with peaks at the corners. However, the standard NASTRAN model peak strain magnitude is significantly less than peak linear elastic response predicted from the test data. This is principally due to the coarse mesh around FFVH #13, where the large strain gradient cannot be captured with relatively large linear elements. The polynomial or 'p' elements used in the enhanced NASTRAN model (Figure 10) overcome the limitation of the standard NASTRAN model and bring a marked improvement to the peak strain results at the FFVH corners.

## 4.2 Strain Distribution Around FFVH #14

Recently concern has been expressed about the stress concentration at FFVH #14, due to the occurrence of a single crack, at this location, in one of the RAAF's F-111s [16]. The causes of any fatigue cracking in FFVH #14 are thought to be similar to those which cause cracking in FFVH #13; that is, the large residual tensile stress caused by the CPLT

[3] Multiplied by the correlation factor, 1.059 [6].

coupled with the flight loading at a hole which acts as a stress concentrator. It should be noted that any further work on developing and assessing a rework profile for FFVH #14, (similar to that previously completed for FFVH #13), will require a FE model that can accurately predict both the peak strains and the large strain gradients around this hole. The non-zero elastic principle strain or 'hoop strain' results, during maximum positive CPLT loading, around the perimeter of FFVH #14 are presented in Figure 15. The peak hoop strains around FFVH #14 are presented below in Table 9, for both the upper outboard and lower inboard corners, noting that the most recent cracking occurred in the lower inboard corner.

*Table 9: Peak hoop strain ($\varepsilon_{\theta\theta}$) around FFVH #14 at maximum CPLT load*

| Location | FFVH #14 peak strain (με) | | | |
|---|---|---|---|---|
| | Elastic test results | PAFEC results[4] | NASTRAN results | |
| | | | *standard* | *enhanced* |
| Lower inboard corner | -12846 | -16479 | -9221 | -13442 |
| Upper outboard corner | -9777 | -17799 | -6356 | -10724 |

It is clear that the predicted elastic PAFEC model peak strains are significantly larger than the test values or the NASTRAN peak strain predictions. This lack of precision of the PAFEC model around FFVH #14 could be due to boundary conditions, or the use of 2D elements in a 3D stress field. Some minor improvement may be possible for the upper outboard corner, by increasing the thickness of the stiffener elements towards the upper plate to represent the local shape more accurately, (this was done for FFVH #13 region in prior work). However this change would have negligible effect for the lower inboard corner. The results from the elastic analysis of both the standard and enhanced NASTRAN versions, show a similar strain trend around the perimeter of FFVH #14, with peaks in the corners. As was the case for FFVH #13, the standard NASTRAN model peak strain is significantly less than peak linear elastic response predicted from the test data. Again, the limitation of the standard NASTRAN model is overcome by increasing the element order around the perimeter of FFVH #14, in the enhanced model. This provides results in good agreement with the test data.

## 4.3 Strains in Stiffener #3 Below FFVH #13 and #14

The magnitude and the direction of the principle strains in the stiffener around FFVH #13 and #14 will give a general indication of the load flow, and local boundary conditions to this region. Hence it was decided to compare the FE strains to the experimental results. Here the Stiffener #3 strains below FFVH #13 and #14, refer to the four positions ①,②,③,

[4] Multiplied by the correlation factor, 1.059 [6].

and ④, shown in Figure 11, on both the forward and aft face of the stiffener. PAFEC and NASTRAN FE model results were found for the closest appropriate node to the position of these gauges, as listed in Table 7. Figure 16 and 17 show the horizontal and vertical strains in stiffener #3 below the FFVH #13 and #14 at maximum CPLT load respectively. It can be seen that the PAFEC model, which uses 2D plate elements to model the stiffener, made reasonable estimates of the strains, both on the forward and aft face. The dominant principal stress axis is oriented approximately 16° from the horizontal, so the horizontal strains are significantly larger than the vertical strains, and for convenience these horizontal strains are listed in Table 10. Overall, the NASTRAN model predicts the horizontal and vertical stiffener strains very well, including the trend along the stiffener. It is worth noting that there is very little difference between the standard and enhanced NASTRAN model results, at this location, so only one set of data is presented here.

*Table 10: Horizontal strain ($\varepsilon_{xx}$) in stiffener #3 at maximum CPLT load*

| Gauge locations | Stiffener strain (με) | | | | | |
|---|---|---|---|---|---|---|
| | Elastic test results | | PAFEC results[5] | | Standard NASTRAN[6] results | |
| (see Figure 11) | *Forward face* | *Aft face* | *Forward face* | *Aft face* | *Forward face* | *Aft face* |
| ① Under FFVH #14 | -2878 | -3699 | -3605 | -3052 | -2503 | -3453 |
| ② Between FFVH #14 & #13 | -3429 | -2765 | -3502 | -3434 | -3393 | -3052 |
| ③ Under FFVH #13 | -4762 | -3659 | -4181 | -4044 | -4492 | -3767 |
| ④ Inboard of FFVH #13 | -3318 | -4013 | -4001 | -3971 | -3789 | -3970 |

## 4.4 Strains in the Upper Plate Above FFVH #13 and #14

The upper wing skin strain, directly above the FFVHs, will give a general indication of the local load path and define the magnitude of the local wing skin secondary bending. The secondary bending of the upper plate, directly above FFVH #13 and #14 is of particular interest due to the disparity in the PAFEC and NASTRAN model strain distributions around FFVH #14, as discussed in Section 4.2. Relative strains were determined from the single gauges (or FE nodes) 'on top' and 'underneath' the upper plate, above FFVH #13 and #14, as illustrated in Figure 11. Table 11 shows a summary of these relative strains ratios. It can be seen that the PAFEC results show some disparity against the test results, indicating significantly larger bending in the plate above FFVH #14. This could be the cause of the large strains in the PAFEC model results around the FFVH #14, particularly in the upper outboard corner. Here the simplified plate modelling of the stiffener with 2D plate elements or incorrect boundary conditions

[5] Multiplied by the correlation factor, 1.059 [5].

[6] Standard and enhanced model results are approximately the same, only one set of data presented here.

could be the cause of this discrepancy. The elastic NASTRAN model strain ratios are a very close match to the elastic test data results. This is very promising and indicates that the model overall has enough detail and mesh density to model the secondary plate bending accurately. There is very little difference between the standard and enhanced NASTRAN model results, so only one set of data is presented here.

*Table 11: Relative horizontal strains ($\varepsilon_{xx}/\varepsilon_{xx}$) in upper plate at maximum CPLT load*

| | Relative strain magnitude | | |
|---|---|---|---|
| Definition of gauge locations on plate | Elastic test results | PAFEC results | Standard NASTRAN results[7] |
| on top near FFVH #13 / underneath near FFVH #13 | 0.8595 | 0.8753 | 0.9442 |
| on top near FFVH #14 / underneath near FFVH #14 | 0.7117 | 1.0085 | 0.7636 |
| on top near FFVH #13 / on top near FFVH #14 | 1.0754 | 0.9362 | 1.0979 |
| underneath near FFVH #13 / underneath near FFVH #14 | 0.8904 | 1.0787 | 0.8880 |

# 5. FE Strain Responses Around Stiffener #3

Due to the FFVH#14 strain inconsistencies noted in the previous sections, it was decided to investigate a region more remote of the FFVHs but within the substructure region of the PAFEC model. While the differences between the PAFEC and NASTRAN FE models could possibly be explained by their differences in geometry and modelling techniques, it was subsequently decided to also investigate whether the differences were due to the loading conditions. As discussed in Sections 2 and 3 earlier, the boundary conditions to the PAFEC sub-model, are applied as prescribed displacements from the 'full' wing model, while the NASTRAN loads are applied as a bending moment, shear force and actuator load combination. There is considerable room for error if incorrect boundary conditions are used. Figure 18 and 19 show the locations on the WPF from which FE results were extracted from both models to make a comparison, namely: (i) stiffener #3 inboard and outboard of the chordwise stiffener, and (ii) the upper plate forward and aft of stiffener #3. It should be noted that no test results were available for these regions.

[7] Standard and enhanced model results are approximately the same, only one set of data presented here.

Again there is very little difference between the standard and enhanced NASTRAN model results, so only one set of data is presented here.

## 5.1 Stiffener #3

Horizontal strains in the stiffener, at maximum CPLT load, from both the PAFEC and NASTRAN FE models inboard of FFVH #13, are given in Figure 20. Here the position y=0 on the graph coincides with the top of the stiffener, at the inner surface of the upper plate. At this location the PAFEC model predicts a lower absolute magnitude of horizontal strain than the NASTRAN model. At the bottom of the stiffener, where the titanium shear web bolts to the stiffener, this trend is reversed, with the NASTRAN strain results having a lower magnitude than the PAFEC results. There is also a noticeable difference in trend through the stiffener. The PAFEC model predicts that the magnitude of the horizontal strains will be approximately the same along the stiffener height. The NASTRAN model shows that the horizontal strains are much larger at the top of the stiffener (towards the plate), with an almost linear decrease in magnitude towards the lower edge of the stiffener (towards the web bolts).

Figure 21 shows the horizontal strains from both the PAFEC and NASTRAN FE models at the position outboard of FFVH #14 and the chordwise stiffener. Unfortunately the mesh density is low in this region, and this is reflected in the results. For both the NASTRAN and PAFEC FE models, the stiffener strains through the plate have similar magnitudes, with the horizontal strain at the top of the plate being of a higher magnitude than that at the bottom of the plate, but the overall trend of the two models is considerably different. In Figure 20 and 21, the variation through the thickness of the stiffener is also significant at some positions. The overall discrepancies between the two models could be due to the different modelling techniques, PAFEC has 8 noded 2D plate elements, and the NASTRAN model has 8 noded 3D elements. The disparity in stiffener strains results from the two models indicates that there are differences in the stiffener bending, again this could be due to the differences in geometry, or in the boundary conditions, for example load transfer at the bolt locations. As a further comparison, Figure 22 and 23 show contour plots of the horizontal strain predictions for both models. The contour plots are relatively similar, showing the regions of high strain at the bolts and around the FFVHs.

## 5.2 Upper Plate

Unaveraged (through-thickness) strains for the upper plate above stiffeners #2 and #4 are given in Figure 24 and 25 respectively. Here the far right side of the graph corresponds to the inboard position, on the wing pivot hub. There appears to be very little difference in the NASTRAN and PAFEC models' strain results in the upper plate along stiffeners #2 and #4. At the inboard edge (far right of graph) there is a small difference between the elastic strains in the upper plate along stiffener #2 in the xx (inboard/outboard) and zz (fwd/aft) directions. This difference could be due to the discrepancies in alignment of

the FE models in its local axis system. Figure 26 and 27 show the averaged (through the thickness) strains along upper plate between stiffeners #2 and #3 and between stiffeners #3 and #4 respectively. Again, the far right side of the graph corresponds to the inboard position, on the wing pivot hub. As was the case with the two previous figures, there is little difference in the upper plate strains, spanwise along the model, between stiffeners #2, #3 and #4. Only between stiffeners #2 and #3 are there any notable but small differences between strain results from the PAFEC and NASTRAN results, where the PAFEC strain magnitudes in the xx direction near the hub are slightly lower than those in the NASTRAN results.

The predicted elastic average strains, along the upper plate parallel and outboard of the chordwise stiffener, are given in Figure 28. There is very little difference between the strain results from the two FE models, but these results are limited by the relatively coarse mesh in this region. Figure 29 shows the unaveraged upper plate strains along stiffener #3 from both the PAFEC and NASTRAN FE models. In these results there are a significant difference, in particular the strain in the zz direction (forward/aft). The PAFEC strains in the region around FFVH #13 and #14 show a very different trend from the NASTRAN results. The PAFEC strains immediately outboard of FFVH #14 are greater than the NASTRAN strains, while just inboard of the hole they are less. This trend is repeated around FFVH #13. Contour plots of transverse strain (forward/aft) in the upper plate from the PAFEC and NASTRAN FE models are given in Figure 30 and 31 respectively. Again in the contour plots the variation of strain around the FFVHs is noticeably different, with the PAFEC model displaying large values around the inboard corners and smaller values around the outboard corners.

# 6. Conclusions

An appraisal of the current AMRL PAFEC and NASTRAN F-111 WPF FE models was required to assess their suitability for use in structural integrity investigations, relating to elastic notch stress and strain predictions. This includes the possible future development of optimal rework shapes to minimise peak notch stresses. Hence in the present work, a comparison between these model predictions and experimental strain data has been undertaken, focussing primarily on the region in the vicinity of FFVH #13 and #14. The following specific points can be made:

1. The PAFEC model accurately predicts the strain distribution around FFVH #13, which indicates its suitability for use in future applications relating to FFVH #13.

2. The PAFEC model incorrectly predicts significantly higher strains in FFVH #14 and greater bending of the wing skin above FFVH #14, making it at present unsuitable for use in further FFVH #14 analyses. The reason for this discrepancy is not clear, however, it may be due to the use of essentially 2D elements in a 3D stress field.

3. The NASTRAN model gives accurate results for the large stress gradient around FFVH #13 and #14, when higher order 'p' elements are used. It is clear that these elements also provide a powerful indicator for defining the extent to which the model can be improved by remeshing alone.

4. The NASTRAN model accurately predicts the upper plate bending near FFVH #13 and #14.

5. Comparison of the PAFEC and NASTRAN strain predictions for stiffener #3, but removed from FFVH #13 and #14 indicates significant differences. This may be due to differences in model geometry, or due to the boundary conditions on the stiffener, (ie loads transferred through the bolts).

6. Overall, it is recommended that further FE analyses of FFVH #13 in the F-111 WPF can be accurately completed with the current PAFEC or NASTRAN model, However only the NASTRAN model is suitable at FFVH#14, and it is the recommended model for general elastic structral integrity assessments, and continued development where appropriate.

# 7. Acknowledgments

The authors wish to acknowledge the helpful comments provided by Mr K. C. Watters, Mr J. Paul, Mr M. McDonald and Mr F. Moras.

# 8. References

1. **CRUMP, G. R. (1970)** Test Loads and General Procedures for the F-111 Proof Test Program, General Dynamics Report FZS-12308B, Fort Worth, USA.
2. **WALKER, K. (1996)** Improved Electrical Discharge Machining Procedures for Re-work of Fuel Flow Vent Hole no 13 in F-111 Wing Pivot Fitting, Structures Laboratory Report No 9/96, Airframes and Engines Division, Aeronautical and Maritime Research Laboratory, Melbourne, Australia.
3. **WATTERS, K. (1997)** Strain Surveys of Fuel Flow Vent Hole Number 13 and Stiffener Runout Number 2 in the F-111 Wing Pivot Fitting for a Range of Rework Shapes. DSTO-TR-0567, DSTO Aeronautical and Maritime Research Laboratory, Melbourne, Australia.

4. **PAUL, J., CHAPMAN, P. and SEARL A. (1996)** Elastic/Plastic Finite Element Analysis of the F-111 Fuel Flow Vent Hole Number 13, DSTO-TR-0454, DSTO Aeronautical and Maritime Research Laboratory, Melbourne, Australia.

5. **McDONALD, M., MAAN, N. and MORAS, F.** Validation and Enhancement of the F-111 Wing Pivot Fitting NASTRAN Finite Element Model, Draft Report M1/9/772, DSTO Aeronautical and Maritime Research Laboratory, Melbourne, Australia.

6. **PAUL, J.** Personal communication regarding correlation factors for PAFEC finite element results, April 1998.

7. **BURCHILL, M. and WATTERS, K.** Correlation of FFVH #14 of the F-111 WPF FE model against test data, Draft Technical Note, DSTO Aeronautical and Maritime Research Laboratory, Melbourne, Australia.

8. **WATTERS, K. C. (1997)** Strain Surveys Fuel Flow Vent Hole Number 13 and Stiffener Runout Number 2 in the F-111 Wing Pivot Fitting for a Range of Rework Shapes, DSTO-TR-0567, DSTO Aeronautical and Maritime Research Laboratory, Melbourne, Australia.

9. **LILLINGSTON, K. (1995)** F-111 Wing Variable Sweep Strain Survey, Structures Laboratory Report 8/95, Airframes and Engines Division, Aeronautical and Maritime Research Laboratory, Melbourne, Australia.

10. **SWANTON, G. (1996)** F-111 FFVH#13 Intermediate Rework Strain Survey, Structures Laboratory Report 6/96, Airframes and Engines Division, Aeronautical and Maritime Research Laboratory, Melbourne, Australia.

11. **WATTERS, K. C. (1997)** F-111 Large Rework Strain Survey, Structures Laboratory Report 7/96, Airframes and Engines Division, Aeronautical and Maritime Research Laboratory, Melbourne, Australia.

12. **ANDERSON, L., FERRAROTTO, P. and SMITH, D. (1990)** Strain Survey of an F111 C Wing Pivot Fitting, ARL-STRUC-TM-523, DSTO Aeronautical and Maritime Research Laboratory, Melbourne, Australia.

13. **MOLENT, L. and SWANTON, G. (1993)** F-111 Fuel Vent Hole #13 Strain Surveys, ARL-TN-33, DSTO Aeronautical and Maritime Research Laboratory, Melbourne, Australia.

14. **LOMBARDO, D. C., PIPERIAS, P., PATTERSON, A. K., FERRAROTTO, P. and SMITH, D. (1990)** Preliminary Strain Survey on F-111C Aircraft A8-113, ARLSTRUC-TM-566, DSTO Aeronautical and Maritime Research Laboratory, Melbourne, Australia.

15. **MOLENT, L. and PATTERSON, A. K. (1992)** Strain Survey of F-111 Aircraft A8-113, ARL-STRUC-TM-585, DSTO Aeronautical and Maritime Research Laboratory, Melbourne, Australia.

16. **WATTERS, K. (1998)** Determination of a rework shape for FVH#14 in F-111 A8-227 right hand wing to remove crack detected during inspection, DSTO Letter Report, B2/03/101 Pt 6 (533), DSTO Aeronautical and Maritime Research Laboratory, Melbourne, Australia.

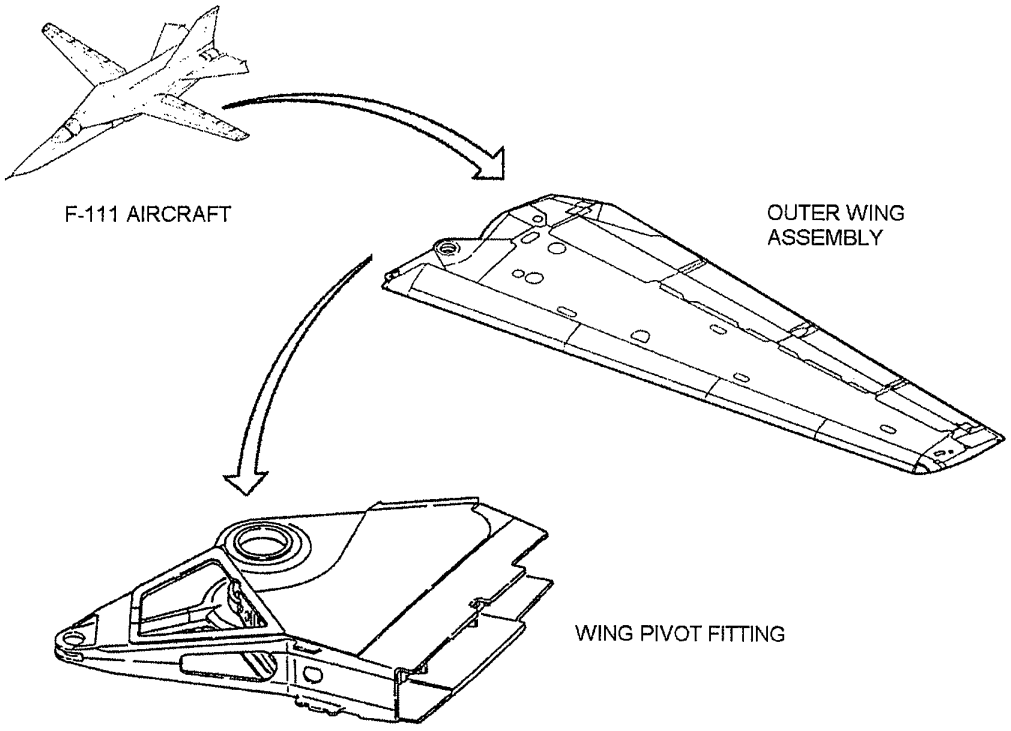


*Figure 1: Overview of the F-111 aircraft showing location of the WPF*

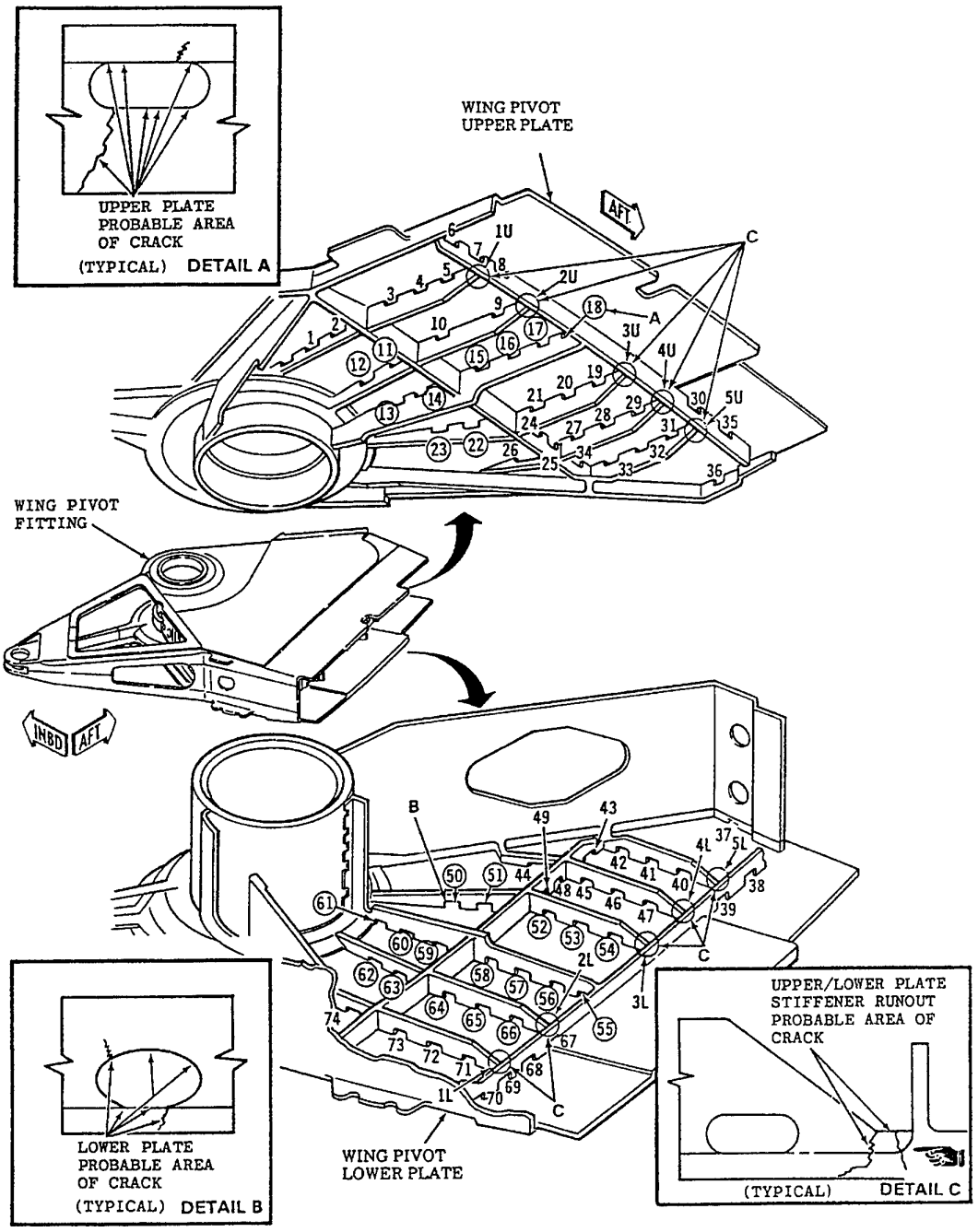


*Figure 2: Internal view of the upper plate of the WPF (showing the FFVH locations)*

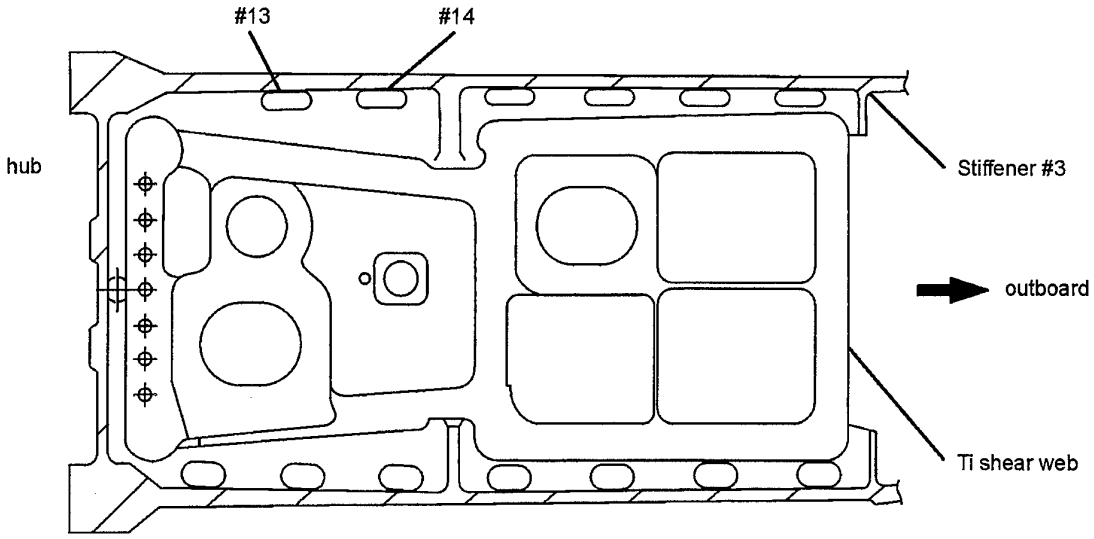


*Figure 3: Section view of WPF along stiffener #3 (showing location of FFVH #13 and #14)*

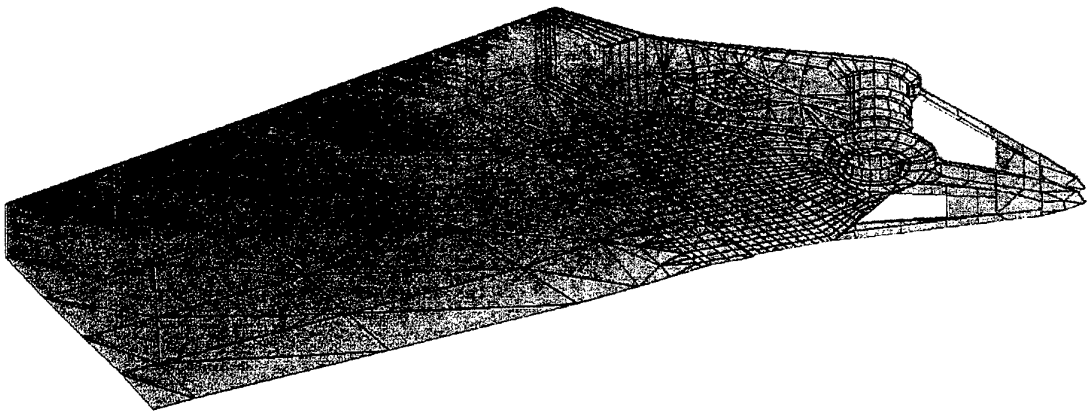

*Figure 4a: PAFEC FE model of F-111 WPF*

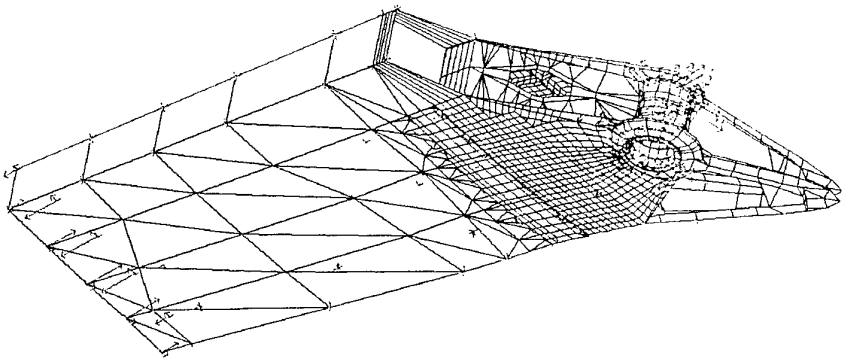

*Figure 4b: Maximum applied load (at 7.33g) to full WPF PAFEC FE model*

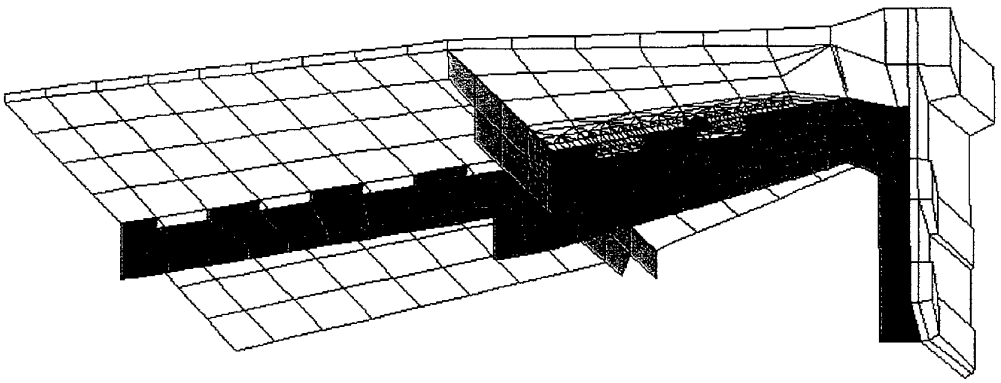

*Figure 5a: Substructure PAFEC FE model*

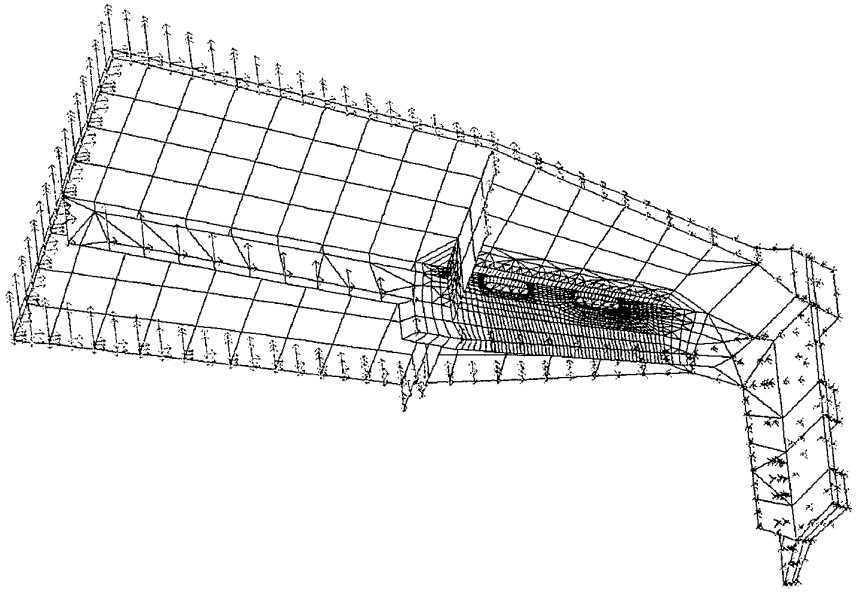

*Figure 5b: Maximum applied displacements (at 7.33g) to substructure PAFEC FE model*

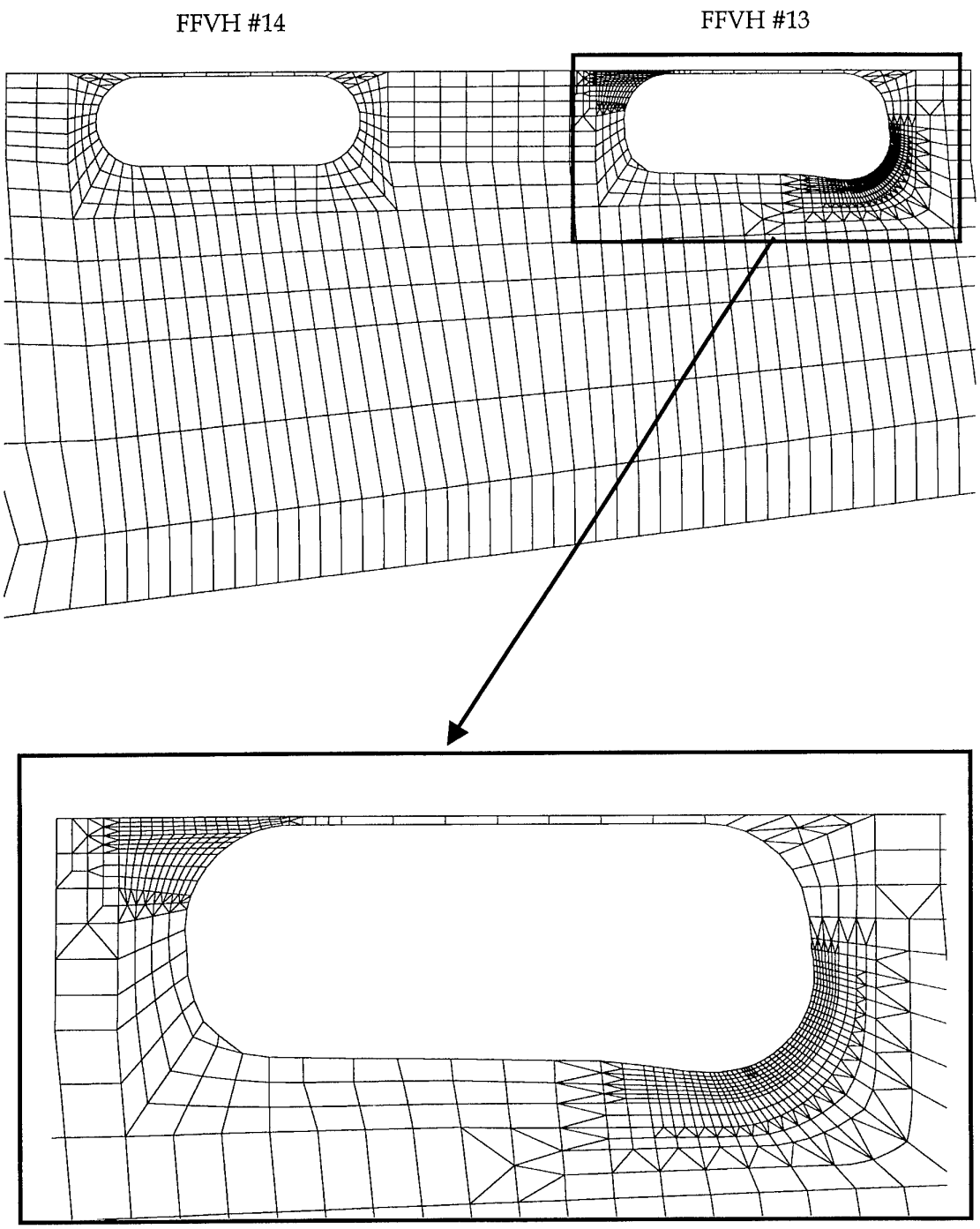


*Figure 6: FFVH #13 & FFVH #14 finite element mesh details in PAFEC model*

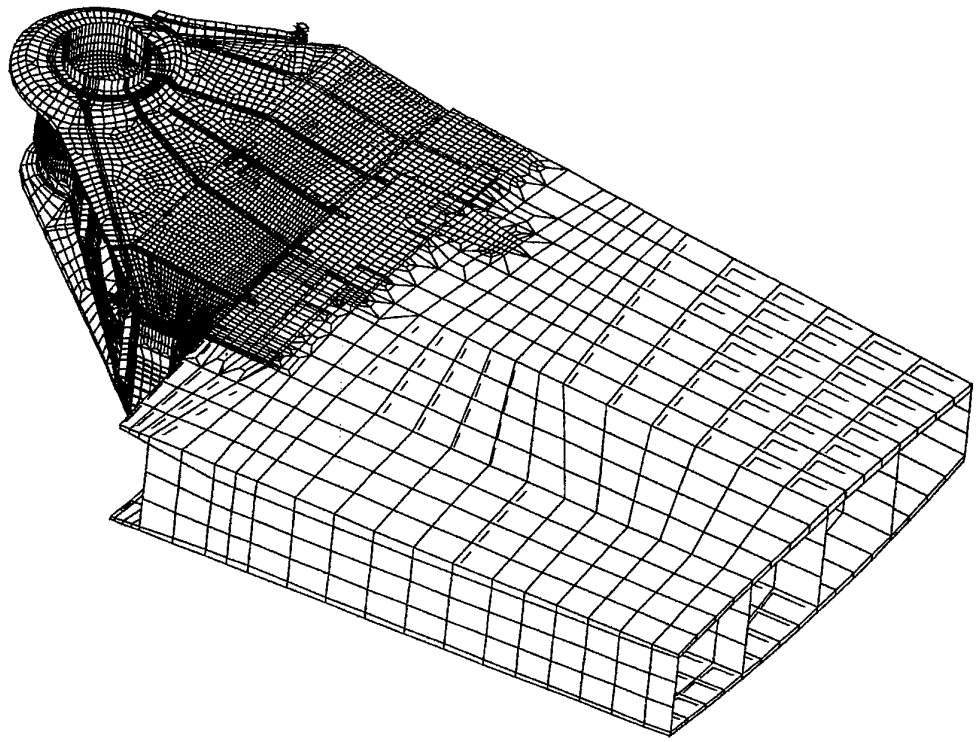

*Figure 7a: NASTRAN FE model of F-111 WPF*

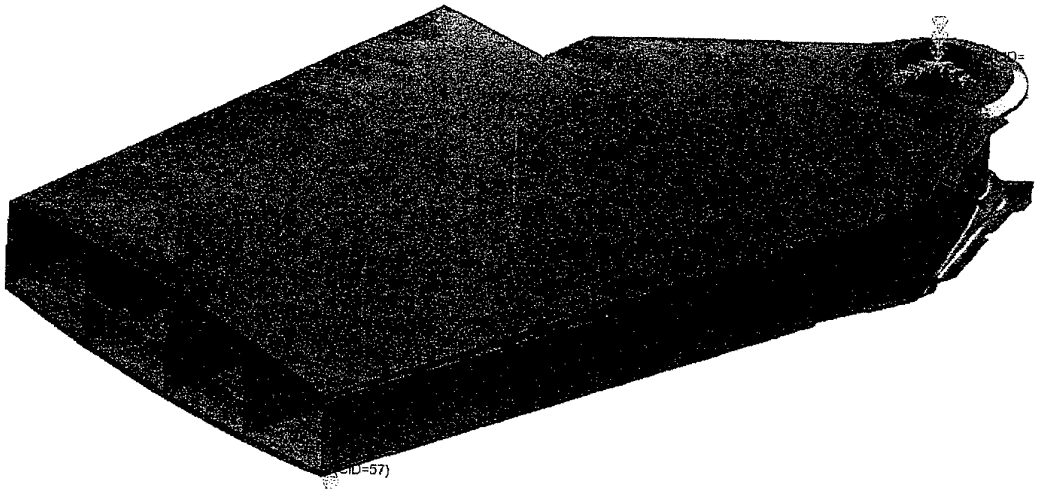

*Figure 7b: Maximum applied load (at 7.33g) to NASTRAN FE model*

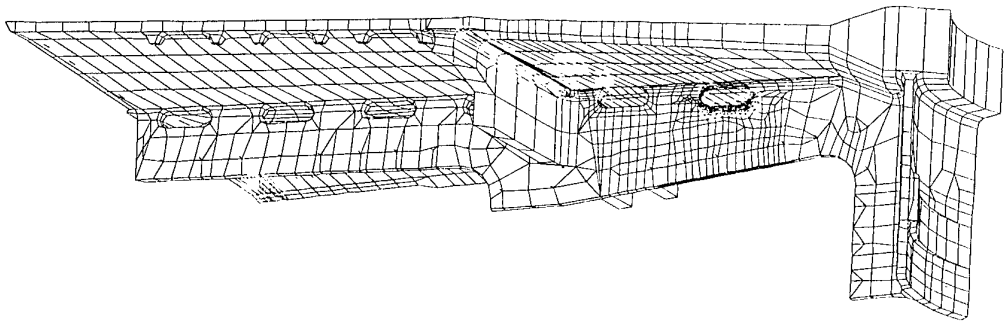

*Figure 8: Stiffener #3 finite element mesh detail in NASTRAN model*

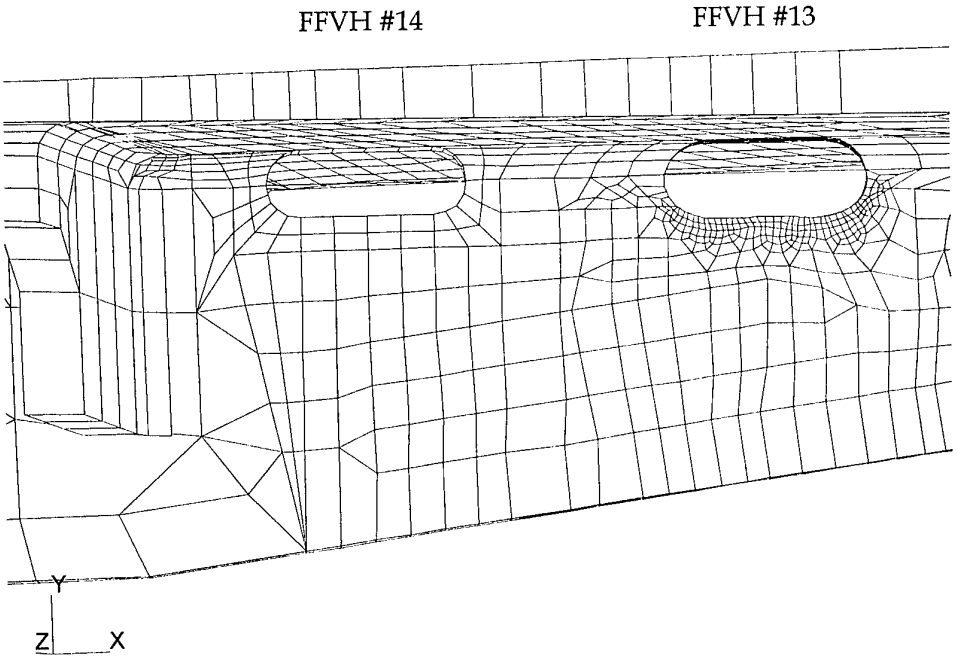


*Figure 9: FFVH #13 & FFVH #14 finite element mesh detail in NASTRAN model*

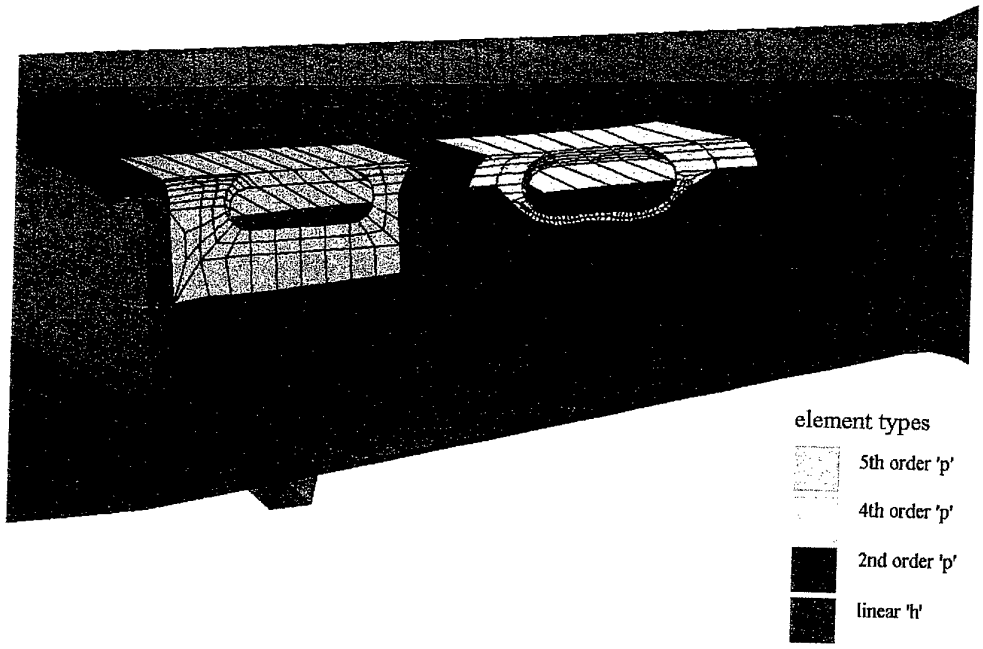


*Figure 10: NASTRAN enhanced model element types*

(i) General arrangement of strain gauges positions (1-12)

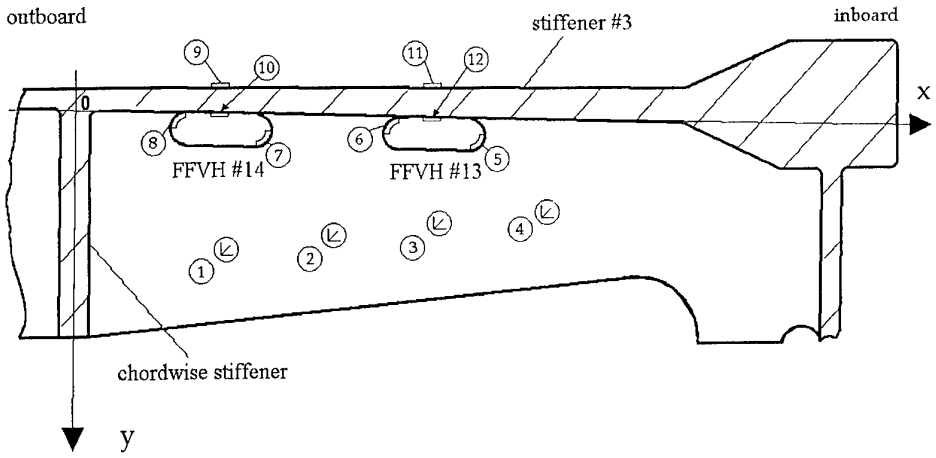


(ii) Location of rosette strain gauges

| Gauge number (aft face/fwd face) | x (mm) | y (mm) | Gauge position |
|---|---|---|---|
| 80/84 | 50 | 37 | 1 |
| 79/83 | 89 | 35 | 2 |
| 78/82 | 126 | 28 | 3 |
| 77/81 | 166 | 22 | 4 |

(iii) Location of strip strain gauges

approximate positions of individual gauges in strip :

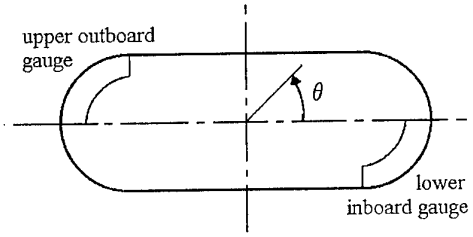


| Gauge strip number | Approximate position of 5 individual gauges in the strip, θ (degrees) | Gauge position |
|---|---|---|
| 72 | 335, 340, 345, 351, 356 | 5 |
| 73 | 155, 160, 165, 171, 176 | 6 |
| 75 | 335, 340, 345, 351, 356 | 7 |
| 76 | 155, 160, 165, 171, 176 | 8 |

(iv) Location of single strain gauges

| Gauge number | Location | Gauge position |
|---|---|---|
| 39 | outside upper plate, above FFVH #14 | 9 |
| 74 | inside upper plate, above FFVH #14 | 10 |
| 38 | outside upper plate, above FFVH #13 | 11 |
| 71 | inside upper plate, above FFVH #13 | 12 |

*Figure 11: Location of strain gauges in the vicinity of FFVH #13 & #14*

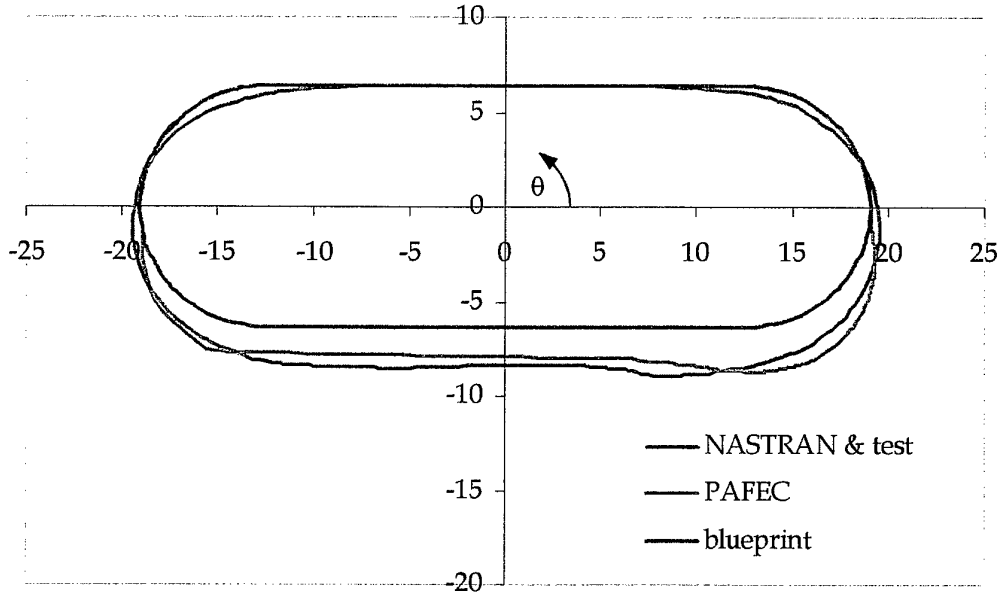


*Figure 12: NASTRAN and PAFEC FE model FFVH #13 profiles*

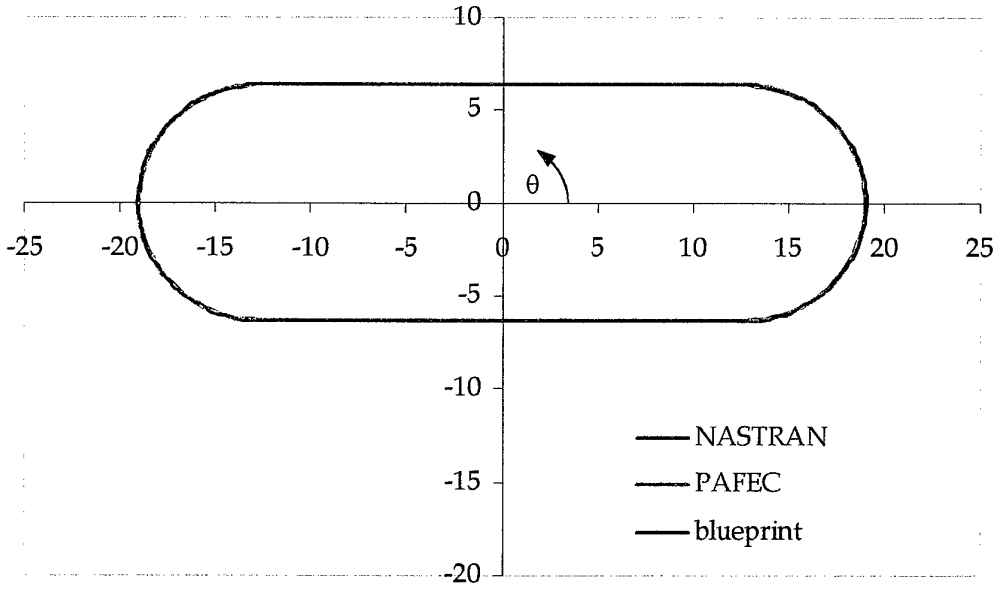


*Figure 13: NASTRAN and PAFEC FE model FFVH #14 profiles*

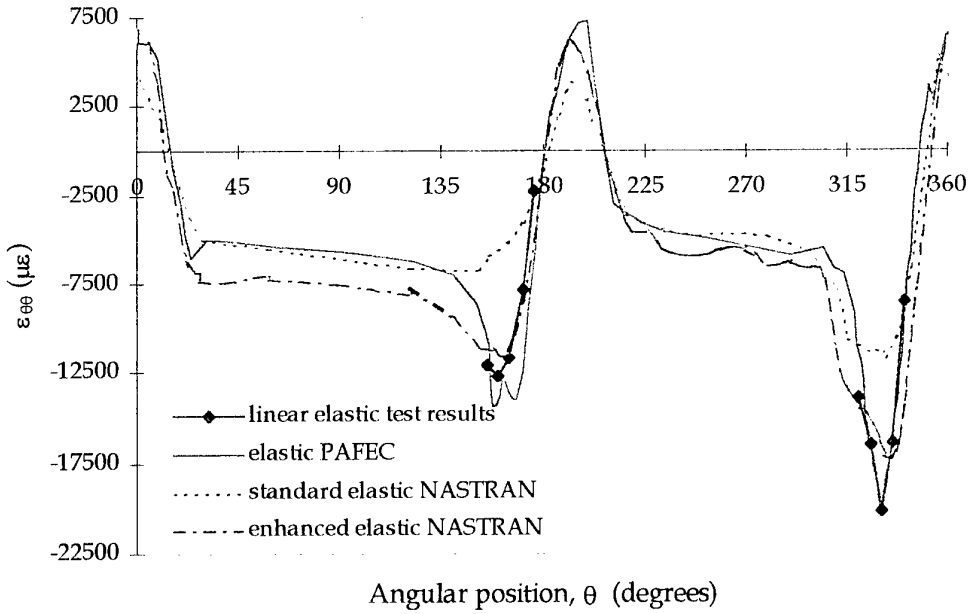


*Figure 14: Comparison of hoop strain around FFVH #13 boundary at maximum CPLT load*

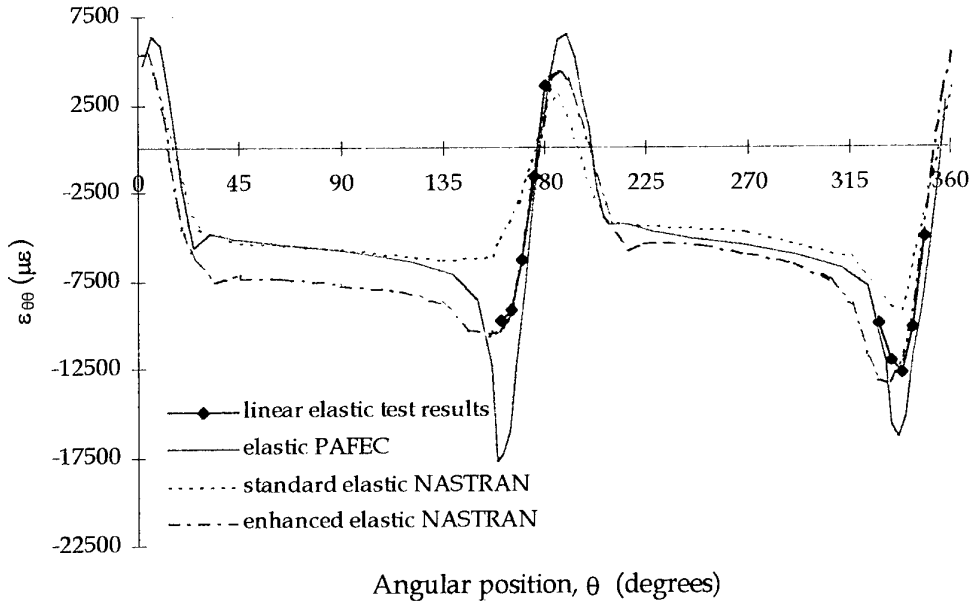


*Figure 15: Comparison of hoop strain around FFVH #14 boundary at maximum CPLT load*

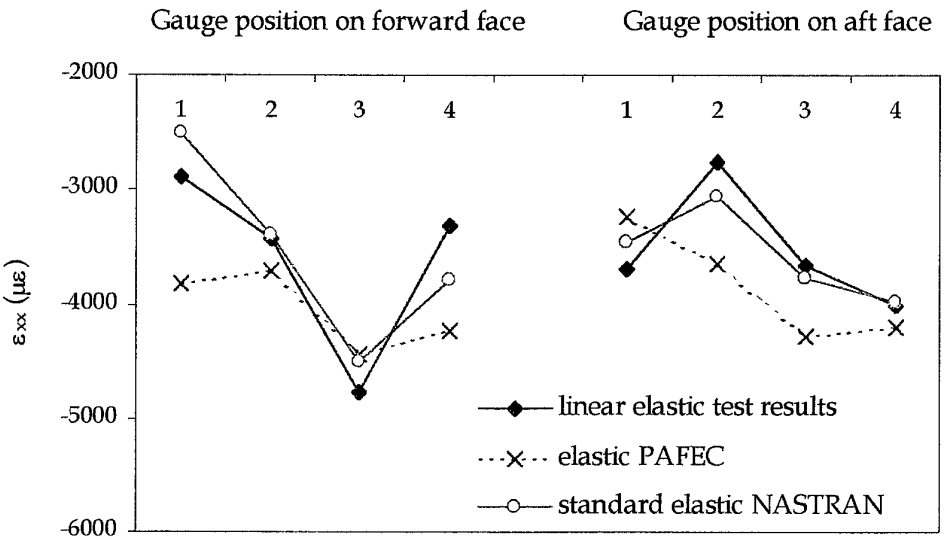


*Figure 16: Comparison of horizontal strain in stiffener #3 at maximum CPLT load*

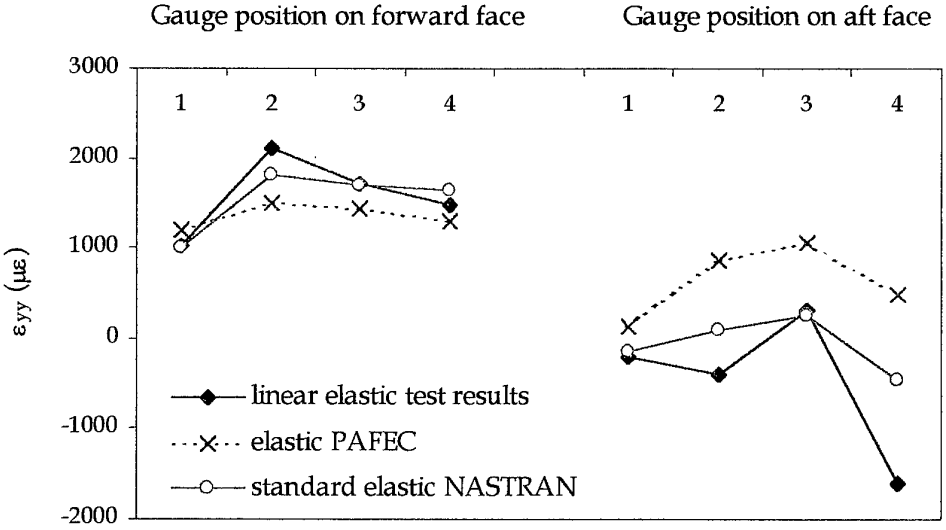


*Figure 17: Comparison of vertical strain in stiffener #3 at maximum CPLT load*

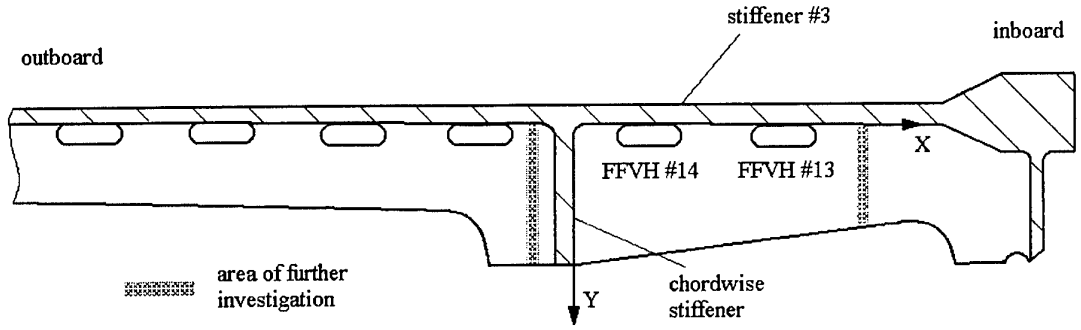


*Figure 18: Locations in stiffener #3 for further detailed comparisons*

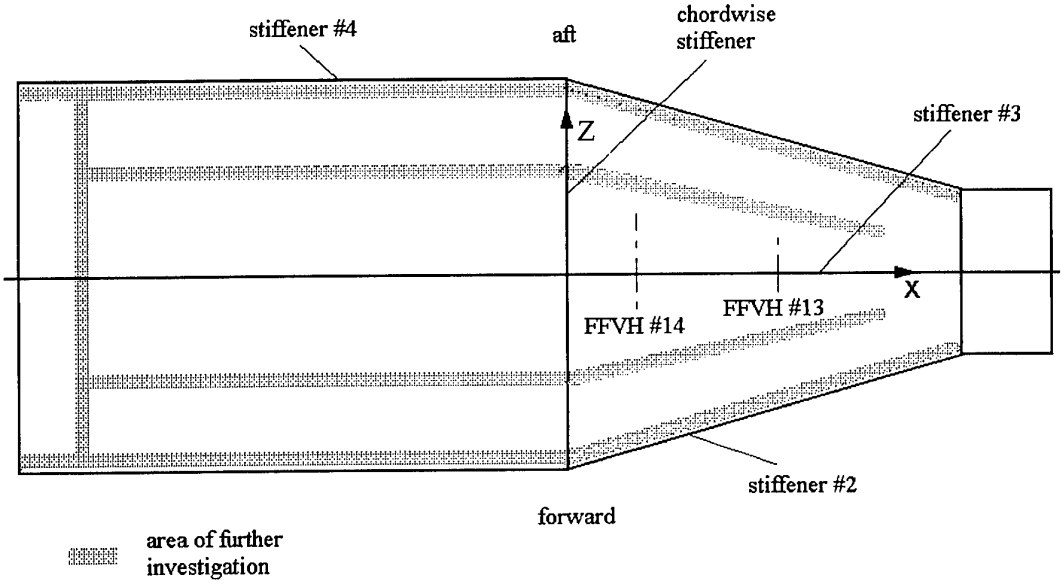


*Figure 19: Locations in upper plate for further detailed comparisons*

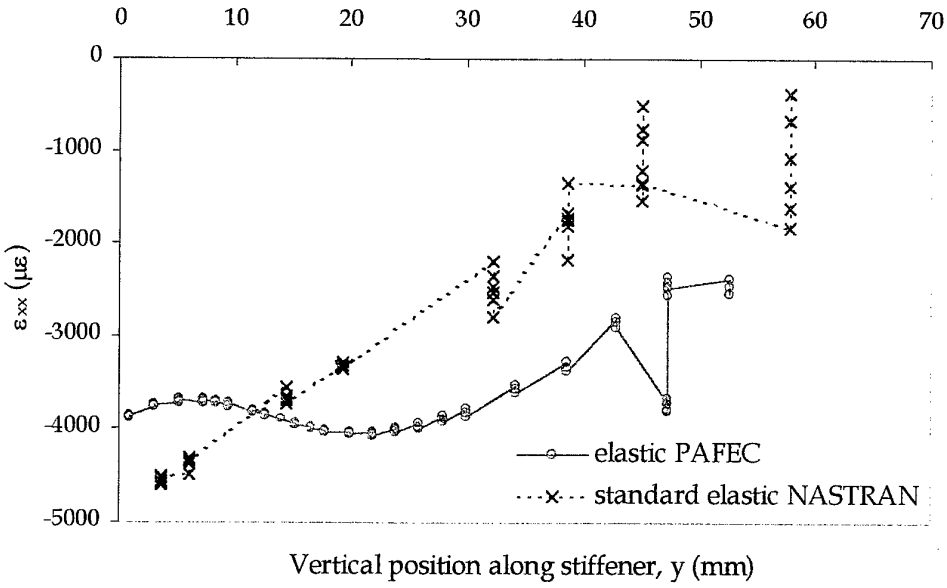


*Figure 20: Comparison of horizontal strain in stiffener #3 inboard of FFVH #13 at maximum*

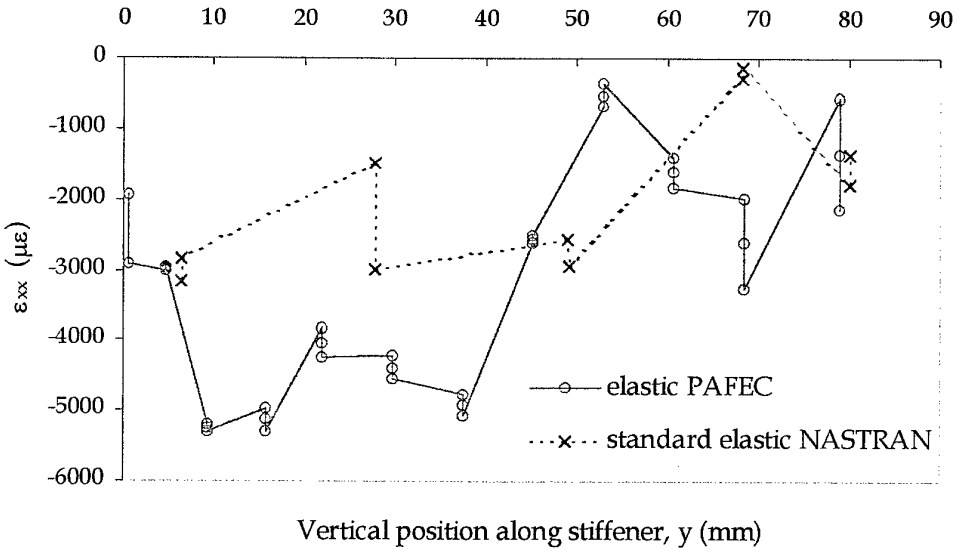


*CPLT load*

*Figure 21: Comparison of horizontal strain in stiffener #3 outboard of FFVH #14 at maximum CPLT load*

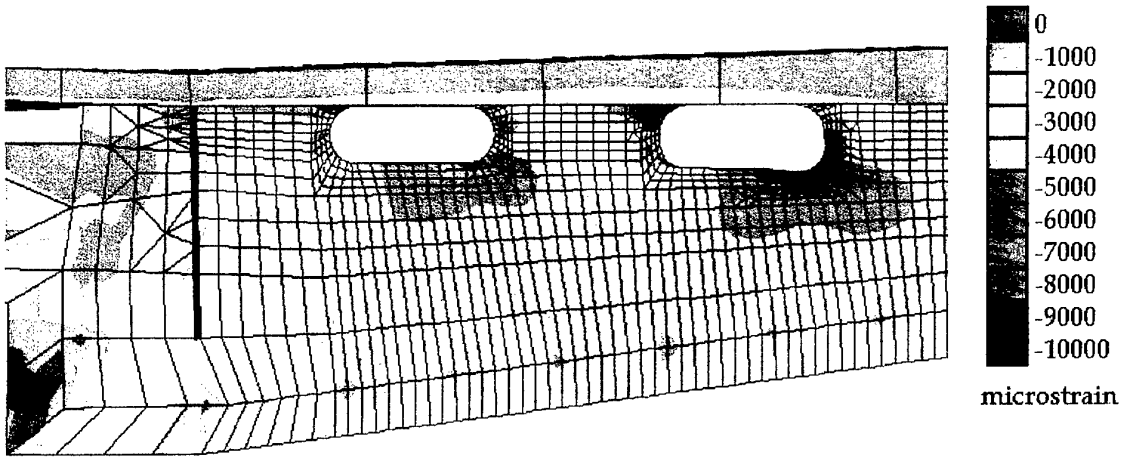


*Figure 22: Contour plot of horizontal strain (εxx) in stiffener #3 of PAFEC FE model at maximum CPLT load*

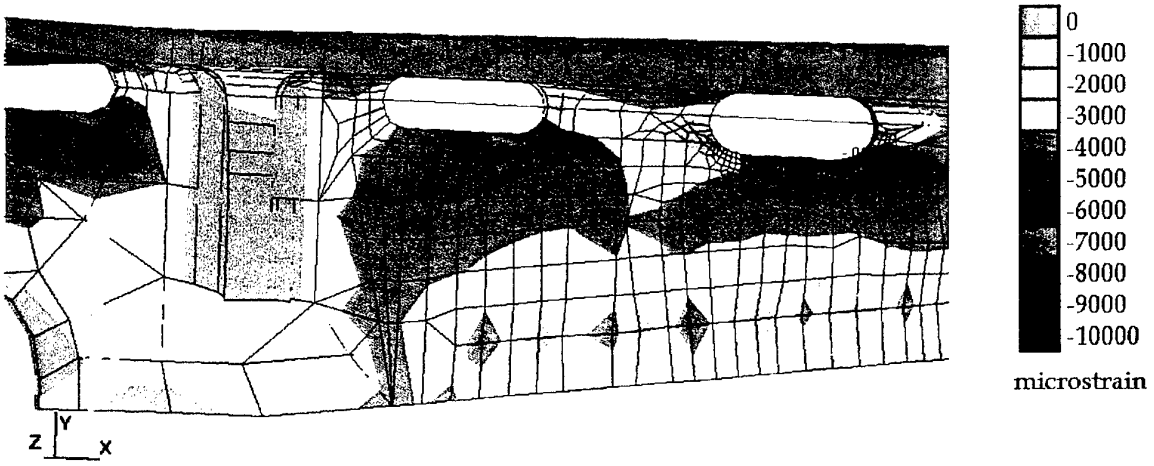


*Figure 23: Contour plot of horizontal strain (εxx) in stiffener #3 of NASTRAN FE model at maximum CPLT load*

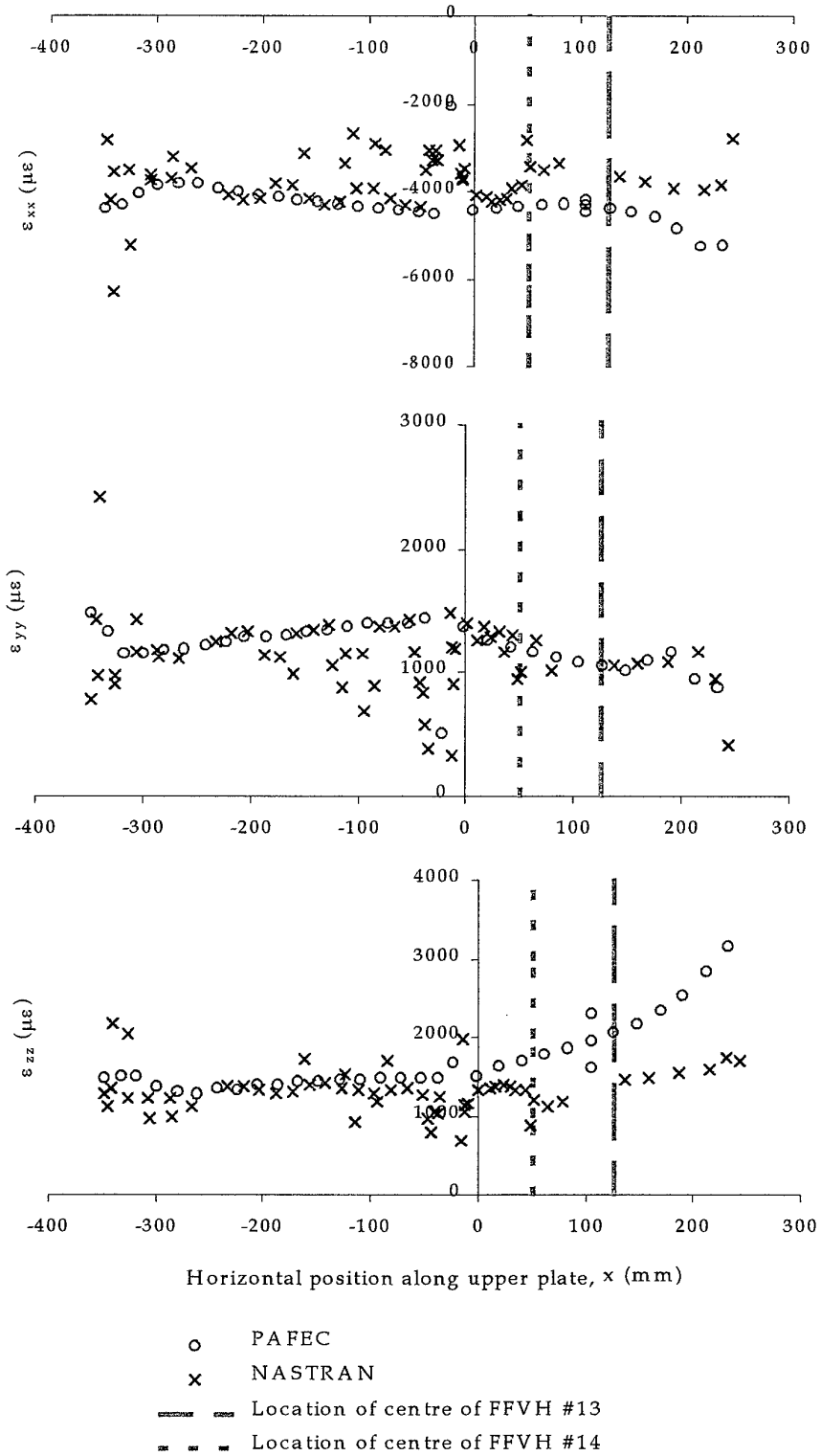


*Figure 24: Unaveraged nodal strains in upper plate above stiffener #2 at maximum CPLT load*

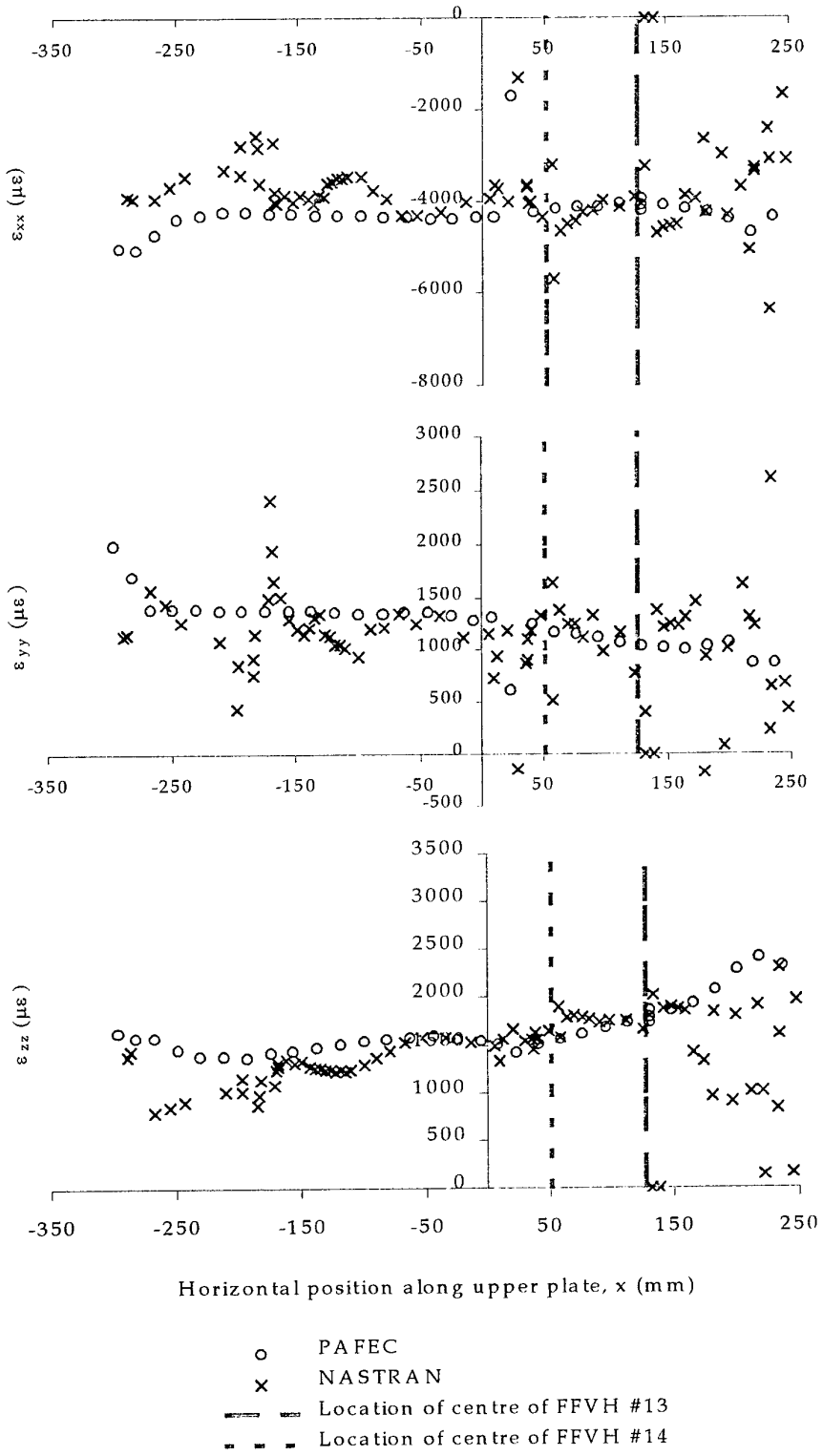


*Figure 25: Unaveraged nodal strains in upper plate above stiffener #4 at maximum CPLT load*

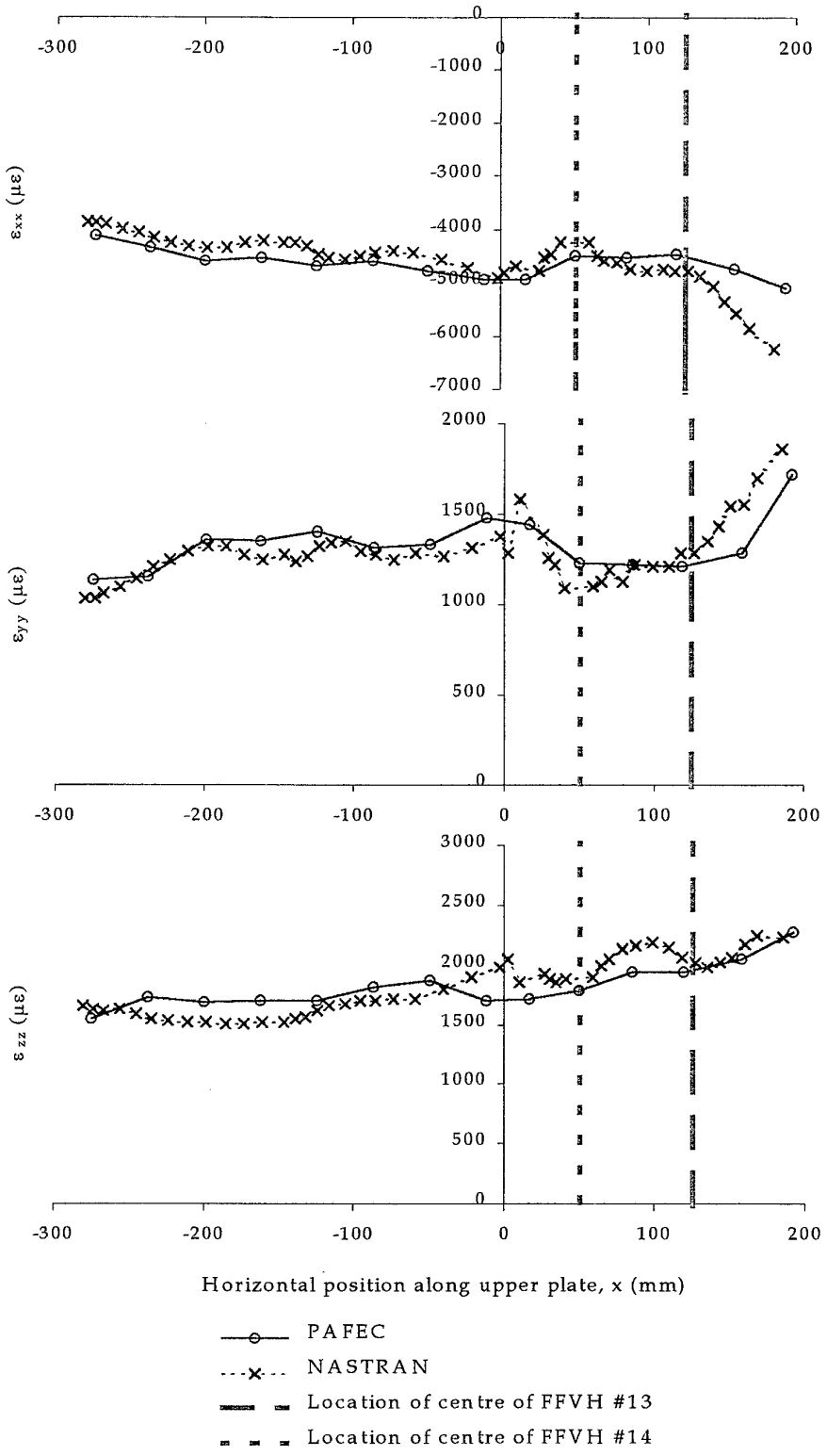


*Figure 26: Averaged nodal strains in upper plate between stiffener #2 and stiffener #3 at maximum CPLT load*

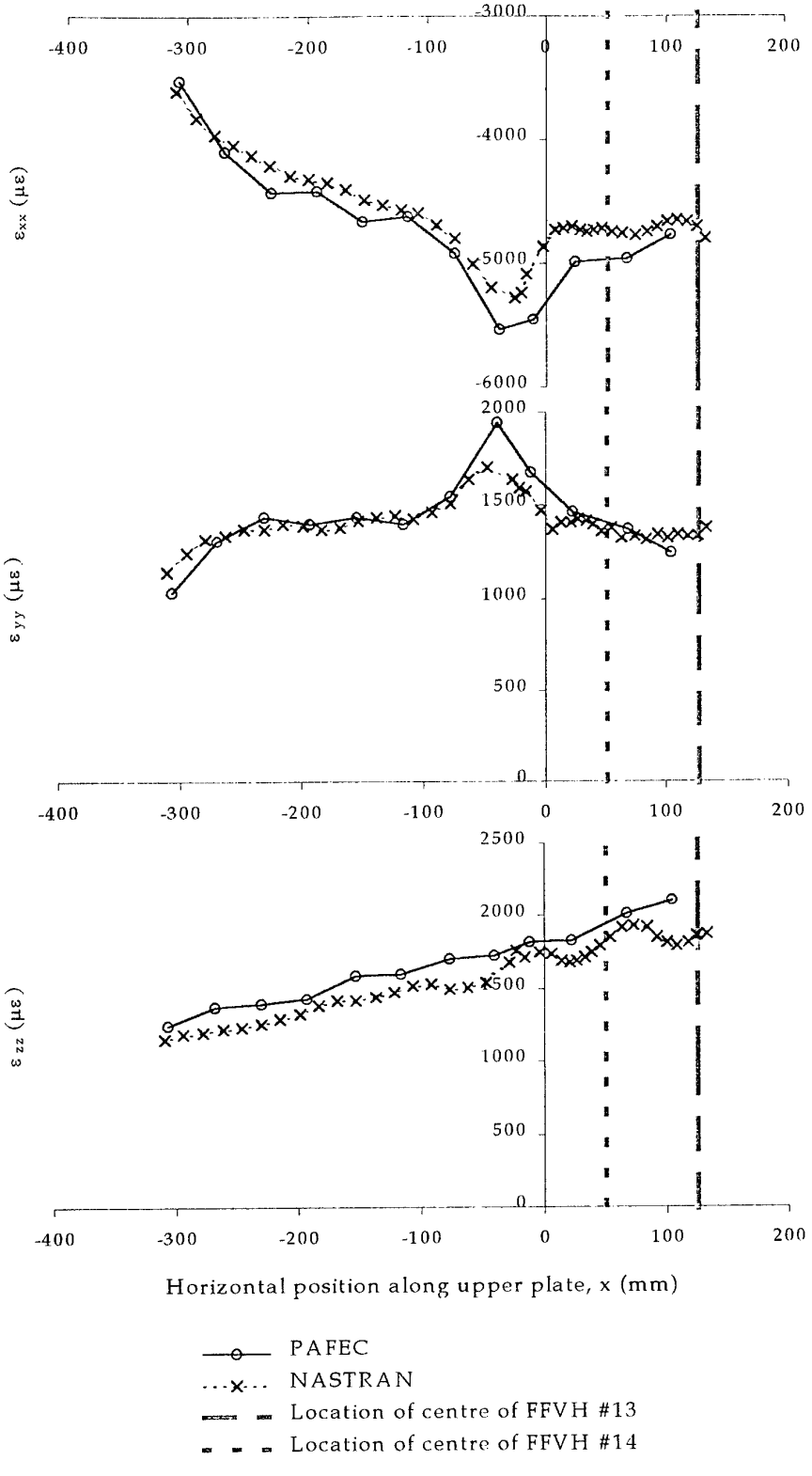


*Figure 27: Averaged nodal strains in upper plate between stiffener #3 and stiffener #4 at maximum CPLT load*

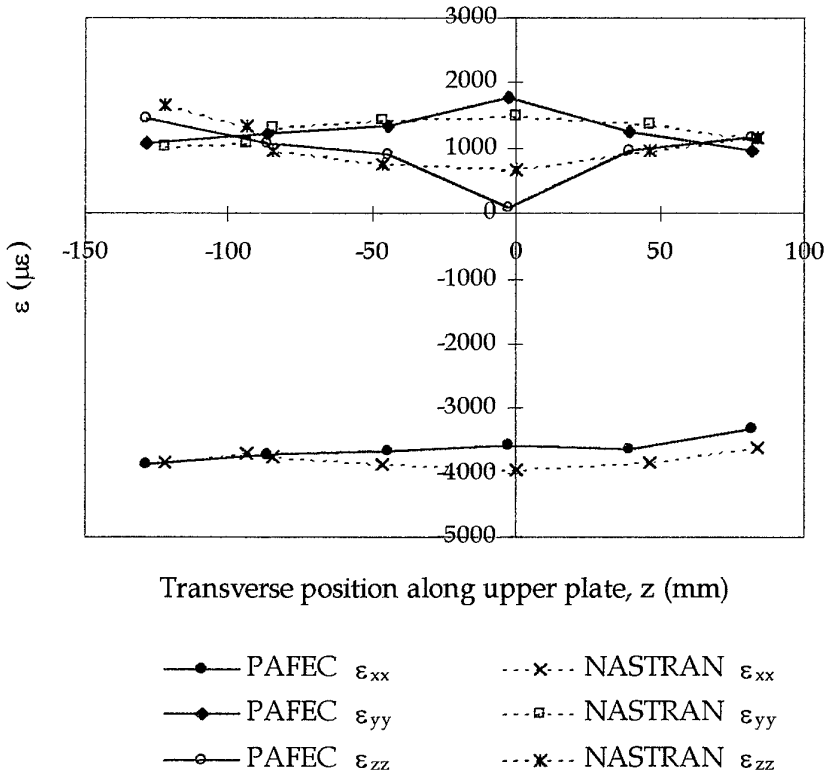


*Figure 28: Averaged nodal strains in upper plate outboard of FFVH #13 at maximum CPLT load*

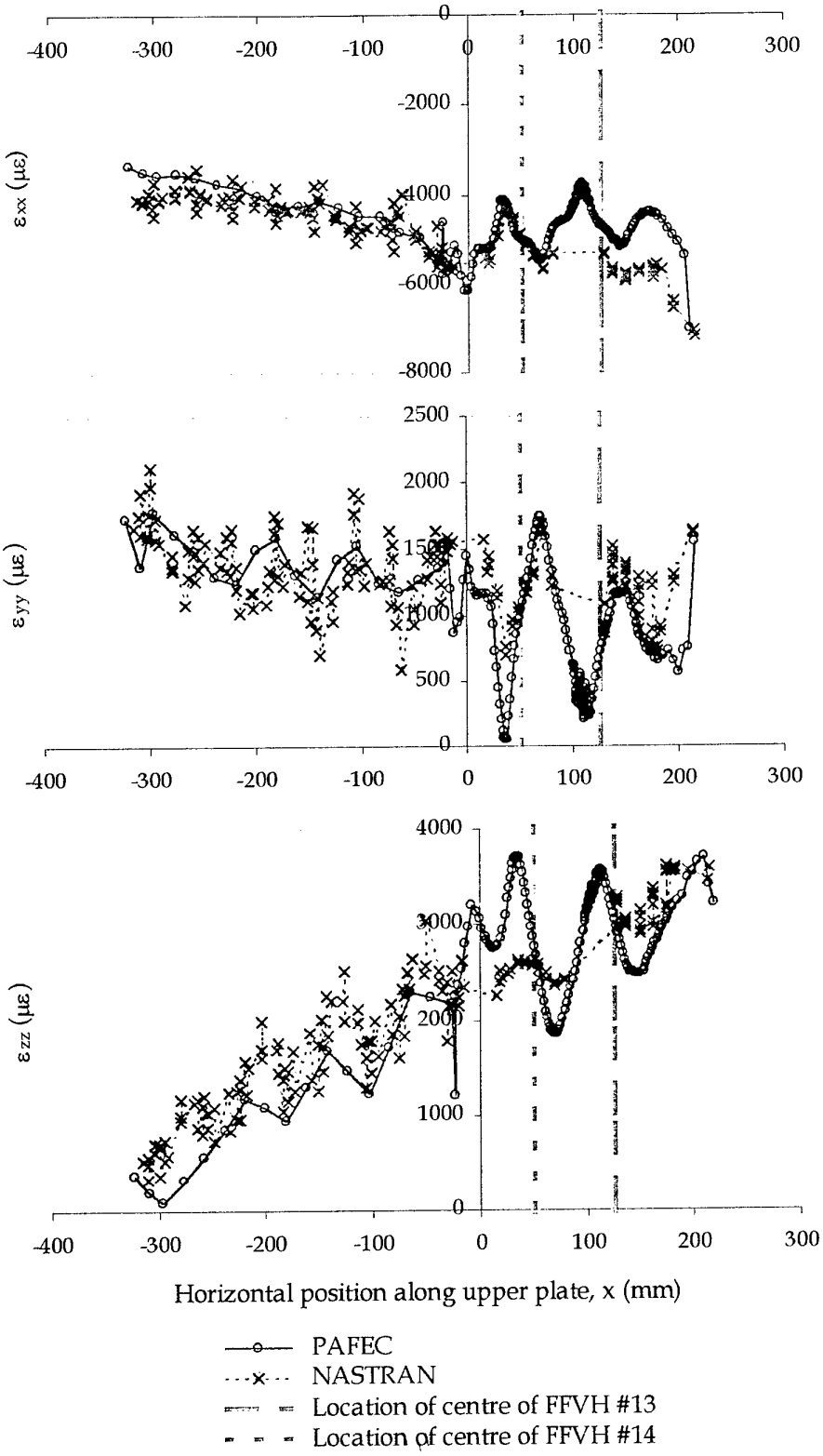


*Figure 29: Averaged nodal strains in upper plate above stiffener #3 at maximum CPLT load*

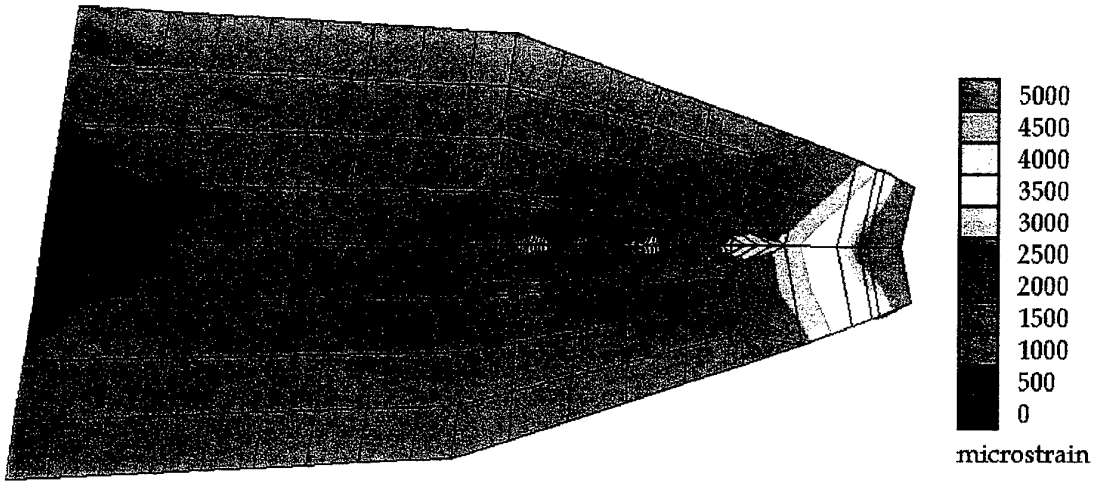


*Figure 30: Contour plot of transverse strain (εzz) in upper plate of PAFEC FE model at maximum CPLT load*

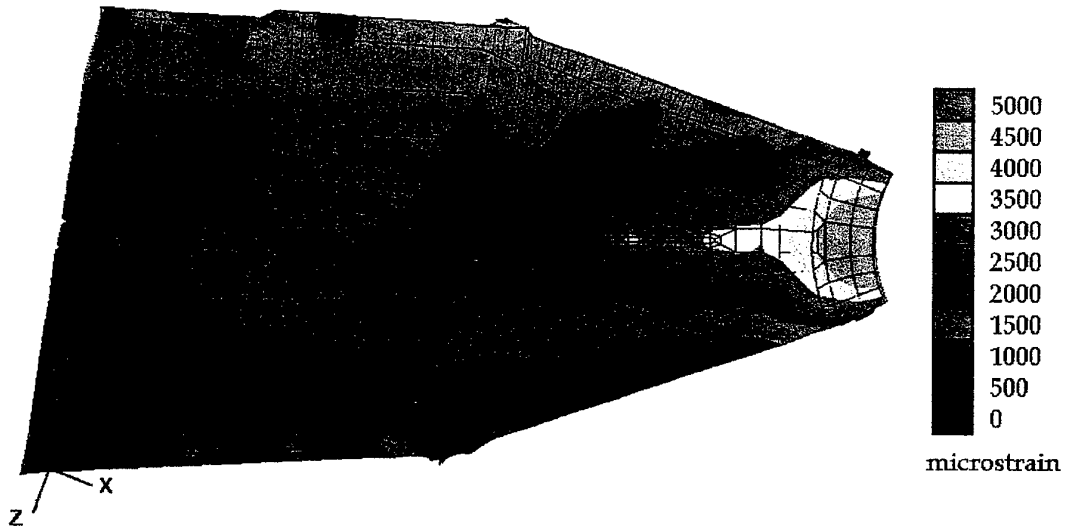


*Figure 31: Contour plot of transverse strain (εzz) in upper plate of NASTRAN FE model at maximum CPLT load*

DISTRIBUTION LIST

Assessment of NASTRAN and PAFEC F-111 WPF FE Models for Elastic Notch Strain Determination at FFVH #13 and FFVH #14

M. Burchill and M. Heller

**AUSTRALIA**

**DEFENCE ORGANISATION**

**Task Sponsor**
DGTA
**S&T Program**
Chief Defence Scientist
FAS Science Policy } shared copy
AS Science Corporate Management
Director General Science Policy Development
Counsellor Defence Science, London (Doc Data Sheet )
Counsellor Defence Science, Washington (Doc Data Sheet )
Scientific Adviser to MRDC Thailand (Doc Data Sheet )
Scientific Adviser Policy and Command
Navy Scientific Adviser (Doc Data Sheet and distribution list only)
Scientific Adviser - Army (Doc Data Sheet and distribution list only)
Air Force Scientific Adviser
Director Trials

**Aeronautical and Maritime Research Laboratory**
Director

Chief of Airframes & Engines Division
Research Leader Fracture Mechanics
Research Leader Structural Integrity
Research Leader Aerospace Composites
Task Manager, K. C. Watters
M. Burchill (4 copies)
M. Heller (4 copies)
M. McDonald
S. Weller
K. Walker
R. Kaye
W. Waldman

**DSTO Library and Archives**
Library Fishermans Bend
Library Maribyrnong
Library Salisbury (2 copies)
Australian Archives
Library, MOD, Pyrmont (Doc Data sheet only)
US Defense Technical Information Center, 2 copies
UK Defence Research Information Centre, 2 copies
Canada Defence Scientific Information Service, 1 copy
NZ Defence Information Centre, 1 copy
National Library of Australia, 1 copy

**Capability Systems Staff**
Director General Maritime Development (Doc Data Sheet only)
Director General C3I Development (Doc Data Sheet only)
Director General Aerospace Development

**Army**
ABCA Standardisation Officer, Puckapunyal, (4 copies)
SO (Science), DJFHQ(L), MILPO Enoggera, Queensland 4051 (Doc Data Sheet only)

**Air Force**
OIC ASI
ASI2
ASI2A

**Intelligence Program**
DGSTA Defence Intelligence Organisation
Manager, Information Centre, Defence Intelligence Organisation

**Corporate Support Program**
OIC TRS, Defence Regional Library, Canberra

**UNIVERSITIES AND COLLEGES**
Australian Defence Force Academy
Library
Head of Aerospace and Mechanical Engineering
Serials Section (M list), Deakin University Library, Geelong, 3217
Hargrave Library, Monash University (Doc Data Sheet only)
Librarian, Flinders University

**OTHER ORGANISATIONS**
NASA (Canberra)
Info Australia (formerly AGPS)

**AEROSTRUCTURES TECHNOLOGIES PTY LTD**
General Manager (B. Madley)
F. Moras

## OUTSIDE AUSTRALIA

**ABSTRACTING AND INFORMATION ORGANISATIONS**
Library, Chemical Abstracts Reference Service
Engineering Societies Library, US
Materials Information, Cambridge Scientific Abstracts, US
Documents Librarian, The Center for Research Libraries, US

**INFORMATION EXCHANGE AGREEMENT PARTNERS**
Acquisitions Unit, Science Reference and Information Service, UK
Library - Exchange Desk, National Institute of Standards and Technology, US
National Aerospace Laboratory, Japan
National Aerospace Laboratory, Netherlands

SPARES (5 copies)

**Total number of copies:** **69**

**DEFENCE SCIENCE AND TECHNOLOGY ORGANISATION**
**DOCUMENT CONTROL DATA**

1. PRIVACY MARKING/CAVEAT (OF DOCUMENT)

2. TITLE

Assessment of NASTRAN and PAFEC F-111 WPF FE Models for Elastic Notch Strain Determination at FFVH #13 and FFVH #14

3. SECURITY CLASSIFICATION (FOR UNCLASSIFIED REPORTS THAT ARE LIMITED RELEASE USE (L) NEXT TO DOCUMENT CLASSIFICATION)

| | |
|---|---|
| Document | (U) |
| Title | (U) |
| Abstract | (U) |

4. AUTHOR(S)

M. Burchill and M. Heller

5. CORPORATE AUTHOR

Aeronautical and Maritime Research Laboratory
PO Box 4331
Melbourne Vic 3001 Australia

| 6a. DSTO NUMBER | 6b. AR NUMBER | 6c. TYPE OF REPORT | 7. DOCUMENT DATE |
|---|---|---|---|
| DSTO-TR-0949 | AR-011-233 | Technical Report | March 2000 |

| 8. FILE NUMBER | 9. TASK NUMBER | 10. TASK SPONSOR | 11. NO. OF PAGES | 12. NO. OF REFERENCES |
|---|---|---|---|---|
| M1/9/547 | AIR 96/102 | DGTA | 42 | 17 |

13. URL on the World Wide Web

http://www.dsto.defence.gov.au/corporate/reports/DSTO-TR-0949.pdf

14. RELEASE AUTHORITY

Chief, Airframes and Engines Division

15. SECONDARY RELEASE STATEMENT OF THIS DOCUMENT

*Approved for public release*

OVERSEAS ENQUIRIES OUTSIDE STATED LIMITATIONS SHOULD BE REFERRED THROUGH DOCUMENT EXCHANGE, PO BOX 1500, SALISBURY, SA 5108

16. DELIBERATE ANNOUNCEMENT

No Limitations

17. CASUAL ANNOUNCEMENT Yes

18. DEFTEST DESCRIPTORS

F-111 aircraft, Wing pivot fittings, NASTRAN (computer software), Modelling, Finite element analysis, Elastic properties

19. ABSTRACT

The current AMRL PAFEC and NASTRAN F-111C wing pivot fitting (WPF) finite element (FE) models have been compared to assess their suitability for use in structural integrity investigations, relating to elastic notch strain predictions, at the two critical fuel flow vent holes (FFVHs). Here a comparison is made between the predicted elastic strains and the measured strain data obtained from a full scale wing test. It was found that the PAFEC model accurately predicts the strain distribution around FFVH #13, however it incorrectly predicts significantly higher strains in FFVH #14 and greater bending of the wing skin above FFVH #14. In contrast, the NASTRAN model gives accurate results for the large stress gradient around both FFVH #13 & #14, and upper plate bending, when higher order 'p' elements are used. Hence it is considered that while FE analyses of FFVH #13 in the F-111 WPF can be accurately completed with either the current PAFEC or NASTRAN model, only the latter is suitable at FFVH#14. Hence the NASTRAN model is the recommended model for general elastic WPF structral integrity assessments, and continued development where appropriate.